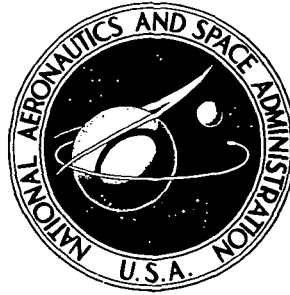


**NASA CONTRACTOR
REPORT**



NASA CR-2510

NASA CR-2510

**VAPORIZATION RESPONSE
OF EVAPORATING DROPS WITH
FINITE THERMAL CONDUCTIVITY**

V. D. Agosta and S. S. Hammer

Prepared by

PROPULSION SCIENCES, INC.

Melville, N.Y. 11746

for Lewis Research Center



1. Report No. NASA CR-2510	2. Government Accession No.	3. Recipient's Catalog No. January 1975	
4. Title and Subtitle VAPORIZATION RESPONSE OF EVAPORATING DROPS WITH FINITE THERMAL CONDUCTIVITY		5. Report Date	
		6. Performing Organization Code	
7. Author(s) V. D. Agosta and S. S. Hammer		8. Performing Organization Report No. None	
		10. Work Unit No.	
9. Performing Organization Name and Address Propulsion Sciences, Inc. P.O. Box 814 Melville, New York 11746		11. Contract or Grant No. NAS 3-16761	
		13. Type of Report and Period Covered Contractor Report	
12. Sponsoring Agency Name and Address National Aeronautics and Space Administration Washington, D.C. 20546		14. Sponsoring Agency Code	
15. Supplementary Notes Final Report. Project Manager, Richard J. Priem, Chemical Energy Division, NASA Lewis Research Center, Cleveland, Ohio			
16. Abstract A numerical computing procedure was developed for calculating vaporization histories of evaporating drops in a combustor in which travelling transverse oscillations occurred. The liquid drop was assumed to have a finite thermal conductivity. The system of equations was solved by using a finite difference method programmed for solution on a high speed digital computer. Oscillations in the ratio of vaporization of an array of repetitively injected drops in the combustor were obtained from summation of individual drop histories. A nonlinear in-phase frequency response factor for the entire vaporization process to oscillations in pressure was evaluated. In addition, a nonlinear out-of-phase response factor, in-phase and out-of-phase harmonic response factors, and a Princeton type "n" and "τ" were determined. The resulting data was correlated and is presented in graphical format. Qualitative agreement with the open literature is obtained in the behavior of the in-phase response factor. Quantitatively, however, the results of the present finite conductivity spray analysis do not correlate with the results of a single drop model.			
17. Key Words (Suggested by Author(s)) Drop vaporization Stability Vaporization response Reynolds process		18. Distribution Statement Unclassified - unlimited STAR category 33	
19. Security Classif. (of this report) Unclassified	20. Security Classif. (of this page) Unclassified	21. No. of Pages 59	22. Price* \$3.75

* For sale by the National Technical Information Service, Springfield, Virginia 22151

VAPORIZATION RESPONSE OF EVAPORATING DROPS

WITH FINITE THERMAL CONDUCTIVITY

by V. D. Agosta and S. S. Hammer

SUMMARY

The primary objective of the analysis was to obtain a numerical computing procedure for determining the vaporization response of droplets with finite thermal conductivity in an oscillating pressure and flow field. The governing equations for vaporization of liquid drops in a rocket combustor environment were taken from Refs. 1 and 2. Additional equations were employed to account for finite thermal conductivity of the liquid drop (Ref. 3). The system of equations were solved utilizing a finite difference technique and a high speed digital computer. Oscillation in the rates of vaporization of an array of repetitively injected drops in the combustor were obtained from the summation of individual drop histories. A nonlinear in-phase frequency response of the entire vaporization process to pressure oscillations was calculated and a response factor, $R_{n\ell}$, was determined as defined by Equation 1 of Ref. 4. In addition, a nonlinear out-of-phase response factor, $I_{n\ell}$, in-phase and out-of-phase harmonic response factors R_1, R_2, I_1, I_2 and a Princeton type "n" and "τ" were determined as described in Refs. 5 and 6. In general, it was found that the nonlinear in-phase response factor, $R_{n\ell}$, was not very sensitive to variations of up to 10^3 in the liquid thermal conductivity, for the frequency range of interest in combustion instability studies.

The resulting data was correlated and is presented in graphical format. Qualitative agreement with the open literature is obtained in the behavior of the in-phase response factor.

INTRODUCTION

Studies on nonlinear combustion instability have been performed (Refs. 2,4,7) which indicate that vaporizing drops are sensitive to frequency-dependent pressure oscillations. The sensitivity of the vaporization processes has been traced to thermal time lags, namely, that time delay between changes in the drop temperature and subsequent mass vaporization and changes in the drop environment. The thermal time lag model proposed in Ref. 7 is extended to include the effects of drop thermal conductivity on drop surface temperature and mass vaporization.

Wave deformation effects on droplet vaporization as proposed in Ref. 5 were also considered in this investigation by varying the harmonic distortion in a pressure disturbance propagating in a liquid rocket combustion chamber.

Nonlinear and harmonic in-phase and out-of-phase response factors which have been evolved from linear limit-cycle stability analyses have been adopted for use in this report. This procedure is consistent with present usage and allows for the comparison of data and results for similar parameters and factors.

THEORY

Drops of liquid oxygen are assumed to be vaporizing in combustion gases, composed of stoichiometric reaction products with hydrogen in a cylindrical combustion chamber, with an established travelling-transverse acoustic mode. The instantaneous pressure and gas velocity functions consist of the steady state and oscillating components attributed to the acoustic mode. They are expressed as

$$p = \bar{p}_c \left(1 + .859 J_1 \left(\frac{1.841 R}{R_w} \right) \right) \left(\frac{\Delta p_1}{\bar{p}_c} \cos(2\pi f t - \theta) + \frac{\Delta p_2}{\bar{p}_c} \cos(4\pi f t - \phi) \right) \quad (1)$$

$$U = [U_a^2 + U_R^2 + U_\theta^2]^{\frac{1}{2}} \quad (2)$$

$$U_R = .430 \frac{a}{\gamma} \left(J_0 \left(\frac{1.841R}{R_w} \right) - J_2 \left(\frac{1.841R}{R_w} \right) \right) \left(\frac{\Delta p_1}{\bar{p}_c} \sin(2\pi ft - \theta) + \frac{\Delta p_2}{\bar{p}_c} \sin(4\pi ft - \varphi) \right) \quad (3)$$

$$U_\theta = .467 \frac{a}{\gamma} \frac{R_w}{R} J_1 \left(\frac{1.841R}{R_w} \right) \left(\frac{\Delta p_1}{\bar{p}_c} \cos(2\pi ft - \theta) + \frac{\Delta p_2}{\bar{p}_c} \cos(4\pi ft - \varphi) \right) \quad (4)$$

$$U_a = U_{a_f} \left(1 - \frac{m}{m_i} \right) \quad (5)$$

where

- a = speed of sound
- f = frequency of oscillations
- J = Bessel function
- m = mass of droplet
- m_i = initial mass of droplet
- p = instantaneous pressure
- \bar{p}_c = mean chamber pressure
- Δp_1 = peak-to-peak pressure amplitude (fundamental)
- Δp_2 = peak-to-peak pressure amplitude (harmonic)
- R = radial location in chamber
- R_N = radius of chamber
- t = time
- T = temperature
- U = gas velocity
- U_{a_f} = final axial gas velocity
- θ = phase angle
- γ = isentropic exponent

The wave is assumed to be adiabatic with chamber temperature and pressure related by

$$\frac{T}{T_c} = \left(\frac{p}{\bar{p}_c} \right)^{\frac{\gamma-1}{\gamma}} \quad (6)$$

The oscillations of pressure and velocity are superimposed on the mean level of parameters affecting drop evaporation and motion. The vaporization rate is controlled by heat and mass transfer to the surface of a drop with finite thermal conductivity. Drop motion is controlled by a momentum balance as a result of drag with the enveloping gas. Axial gas velocity is proportional to the fraction of drop mass vaporized, and it attains a final assumed velocity at complete evaporation. The complete drop history is defined by the following equations for weight evaporation rate, heat transfer, acceleration in an axial direction and temperature distribution within the drop.

The governing differential equation for temperature in a spherical liquid droplet is given by

$$T_t = \alpha(T_{rr} + \frac{2}{r} T_r) \quad \begin{matrix} 0 \leq r \leq r_s \\ t \geq 0 \end{matrix} \quad (7)$$

where α = liquid thermal diffusivity
 r = radial coordinate within the drop
 r_s = surface radius.

The subscripts r and t represent differentiation with respect to radius and time, respectively. For small droplets the assumption of spherical geometry is usually accepted. It is recognized that where drag exists, droplets deform; however, in this analysis the deformation is neglected. The initial condition assumes that the droplet is at uniform temperature T_o ,

$$T(r,0) = T_o \quad 0 \leq r \leq r_s ; t=0 \quad (8)$$

The boundary conditions are

$$T(0,t) \text{ is finite} \quad r=0 ; t \geq 0 \quad (9)$$

and

$$h(T_c - T_s) = kT_r + \frac{\dot{W}}{A_d} [\lambda + c_{pv}(T_c - T_s)] \quad (10)$$

$$r=r_s ; 0 \leq t \leq \infty$$

where h = heat transfer coefficient
 T_s = drop surface temperature
 k = liquid thermal conductivity
 λ = heat of vaporization
 c_{p_v} = specific heat of droplet vapor
 \dot{w} = mass evaporation rate
 A_d = droplet surface area

It is assumed that the film thickness surrounding the droplet is small compared to the droplet diameter.

The mass evaporation is given by

$$\dot{w} = A_d K_g p \ln \frac{p}{p-p_v} \quad r=r_s \quad (11)$$

where p_v = droplet vapor pressure
 K_g = mass transfer coefficient.

The heat and mass transfer coefficients h and K_g , respectively, are obtained from the Nusselt correlations

$$\frac{2r_s h}{k_m} = 2 + 0.6(Pr)^{1/3} (Re)^{1/2} \quad (12)$$

and

$$\frac{2r_s \bar{R}_u T_m K_g}{M_v D} = 2 + 0.6(Sc)^{1/3} (Re)^{1/2} \quad (13)$$

where k_m = vapor-gas mixture thermal conductivity
 \bar{R}_u = universal gas constant
 M_v = molecular weight of vapor
 T_m = arithmetic mean temperature, $\frac{T_c + T_s}{2}$
 Pr = Prandtl number $(c_p \mu / k)_m$
 Sc = Schmidt number $(\mu / D \rho)_m$
 Re = Reynolds number $2r_s (VEL) \left(\frac{\rho}{\mu}\right)_m$
 V_d = drop velocity
 D = molecular diffusion coefficient

and

$$VEL = ((U_a - V_d)^2 + U_r^2 + U_o^2)^{1/2} \quad (14)$$

The droplet acceleration is determined by considering the momentum transfer between the liquid drop and gases due to aerodynamic drag

$$\frac{dv_d}{dt} = \frac{3}{8} C_D \frac{\rho_m}{\rho_l} \frac{(\Delta V) |\Delta V|}{r_s} \quad (15)$$

and the drag coefficient

$$C_D = 27 \frac{2 \rho_m \Delta V r_s^{-.84}}{\mu_m} \quad (16)$$

where ΔV is the difference between the axial gas velocity and drop velocity.

The droplet radius is, of course, a function of time and is related to the mass evaporation rate,

$$\dot{r}_s = \frac{\dot{w}}{\rho_l A_d} \quad (17)$$

where \dot{r}_s = surface regression rate; time rate of change of drop radius.

The analysis of droplet evaporation in a gas stream, as formulated above, is developed into a computer program for the numerical solution of the time dependent evaporation rate, droplet radius and temperature distribution within the drop. A detailed discussion of the calculation procedure and a program listing are contained in Appendix B. Beginning with a specification of the initial conditions the droplet vaporization and surface regression rates are determined from Eqs. (11) and (17). The heat balance equation (10) at the droplet surface is then used to determine the temperature gradient at the surface. By finite difference techniques the temperature gradient at a point adjacent to the surface, and the second derivative of temperature with respect to r at the surface are determined.

Equation (7) is then used to obtain the variation of surface temperature with time. Interior point temperature calculations are performed by utilizing a finite difference scheme for the solution of Eq. (7). At the end of the time interval new values are calculated for surface radius, drop velocity, surface temperature and droplet mass by integrating the appropriate time derivatives over the interval. The gas pressure, temperature and velocity are evaluated at the end of every interval from Eqs. (1)-(6). These thermodynamic and geometric properties then become the initial conditions for the next time interval. The procedure continues until the droplet mass is reduced to 10% of its initial value.

A summation of single-drop histories is used to determine the time variations in vaporization rate of a one-dimensional array of repetitively injected drops. An arbitrary number of drops are injected into the chamber every cycle at times distributed evenly over the oscillation period. For the case of four drops injected per cycle these would appear in the chamber at intervals of one-quarter period. Vaporization histories vary among drops injected at different times during one pressure oscillation; however, drops injected at times one period apart experience identical acoustic pressure and velocity fields and thus, have identical histories. Eventually the same number of drops are completely vaporized per cycle as are injected, and the number of drops in the array becomes constant over each full cycle. When this steady state condition is reached the fully developed array consists of a number of drops equal to the ratio of drop burning time to oscillation period times the number of drops injected per cycle. The droplets in the array have a decreasing mass down the length of the chamber and range in age from a new drop just injected to an old one almost completely vaporized. With the array fully developed, the mass vaporizing from the entire array of drops at any time is obtained from a summation of the vaporization of the individual drops that constitute the array.

Since the history of each injected drop is calculated independently of the preceding or succeeding drops, the computation time is dependent on the number of drops injected per cycle. In order to simulate a continuous injection of drops, it would be necessary to analyze an unwieldy number of drops. Alternatively, it is possible to smooth out perturbations in the array vaporization history caused by the appearance and disappearance of a small finite number of drops by artificially inserting additional drops between those whose histories are calculated. The vaporization rates of the artificially injected drops are determined by interpolation between the vaporization rates of the drops for which calculations are performed. Thus the instantaneous vaporization rate for the entire array is obtained from a summation of the calculated drop histories and interpolated artificial drop histories.

The vaporization history of eight drops, injected at equal intervals during a pressure cycle is shown in Figure 1. The vaporization rate tends to be higher at both the maximum and minimum pressure condition in the oscillation than at the mean pressure conditions. This is a result of lower total velocities at the mean pressure condition. For the case shown in Figure 1, the next drop injected (drop 9) would exhibit the identical behavior as drop 1. For a burning time of .001 seconds and a pressure oscillation period of .00033 seconds the fully developed array would consist of 30 drops with drops 1, 9, 17, 25 exhibiting identical behavior, drops 2, 10, 18, 26 exhibiting identical behavior, etc. The vaporization from the entire array is obtained by adding the evaporation rates of all of the constituent drops at corresponding times in the pressure cycle. The results of this calculation, along with the pressure curve, is shown in Figure 2. It is evident from this curve that the evaporation rate tends to be higher at times in the pressure cycle corresponding to maximum or minimum pressure with relatively lower evaporation rates occurring at the mean pressure.

The calculation shown in Figures 1 and 2 required 160 seconds of computing time on a CDC 6600 computer.

In order to insure that certain computational procedures being used would yield results that were reproducible, the following tests were conducted: In the drop evaporation test runs, calculation was terminated after 90% of the drop mass had evaporated. In order to insure that this was not a premature cutoff point, one run was extended to the 97% mass evaporation point. In the former case, the response function was 0.548; in the latter, 0.545. The difference is negligible; thus a mass termination point of 90% was adopted.

In the determination of the response factor, R_{nl} , eight drops were introduced, evenly spaced during the pressure cycle. The cumulative mass evaporation from these drops was calculated and subsequently the response factor. At low frequencies the drop array size was not statistically meaningful. The question posed was: are eight oxygen drops a statistical meaningful array at a frequency of 1000 Hertz? A quick answer was sought. In one run, 20 drops were used in a drop array and the resulting response factor thus determined did not vary significantly from the results for the eight-drop array.

RESPONSE

Imposing acoustic oscillations on the pressure and velocity field in a rocket combustion chamber causes perturbations in the vaporization rate of the array of droplets resident in the chamber. The oscillation in vaporization rate will exhibit harmonic components of the imposed frequency of acoustic oscillations. A series of response factors are calculated in this study in order to relate vaporization rate oscillations to pressure and velocity field oscillations. These response factors are the in-phase and out-of-phase components of the vaporization rate oscillations relative to the acoustic pressure oscillations, where both oscillations are given as fractional perturbations about the mean value of the variable.

The nonlinear in-phase response factor, R_{nl} , can be extracted from the array vaporization rate and normalized by correlation procedure (Ref. 5) defined by

$$R_{nl} = \frac{\int_0^{2\pi} W' P' dwt}{\int_0^{2\pi} (P')^2 dwt} \quad (18)$$

where

$$P' = \frac{P - \bar{P}_c}{\bar{P}_c}$$

and

$$W' = \frac{W - \bar{W}}{\bar{W}}$$

where W is the instantaneous evaporation rate from the entire array and \bar{W} is the average value of W taken over a full cycle.

The nonlinear out-of-phase response factor, I_{nl} , is given by

$$I_{nl} = \frac{\int_0^{2\pi} W' \sum_{n=1}^{\infty} P_n \sin(2\pi f_n t - \phi_n) dwt}{\int_0^{2\pi} (P')^2 dwt} \quad (19)$$

where

$$P_n = .859 J_1 \left(\frac{1.841 R}{R_w} \right) \frac{\Delta P_n}{\bar{P}_c} \quad (20)$$

Additional response factors were calculated as part of this study:

$$R_1 = \frac{\int_0^{2\pi} W' P_1 \cos(2\pi ft - \theta) dwt}{\int_0^{2\pi} (P_1 \cos(2\pi ft - \theta))^2 dwt} \quad (21)$$

$$R_2 = \frac{\int_0^{2\pi} W' P_2 (\cos 4\pi ft - \varphi) dwt}{\int_0^{2\pi} (P_2 \cos(4\pi ft - \varphi))^2 dwt} \quad (22)$$

Out-of-phase harmonic response factors

$$I_1 = \frac{\int_0^{2\pi} W' P_1 \sin(2\pi ft - \theta) dwt}{\int_0^{2\pi} (P_2 \sin(2\pi ft - \theta))^2 dwt} \quad (23)$$

$$I_2 = \frac{\int_0^{2\pi} W' P_2 \sin(4\pi ft - \theta) dwt}{\int_0^{2\pi} (P_2 \sin(4\pi ft - \theta))^2 dwt} \quad (24)$$

A Princeton type "n" and "τ" defined in Ref. 6 are also calculated from the nonlinear response factors

$$"n" = \frac{R_{nl} (P_1^2 + P_2^2)}{P_1^2 (1 - \cos 2\pi f\tau) + P_2^2 (1 - \cos 4\pi f\tau)} \quad (25)$$

where τ is defined from the following equation:

$$\frac{P_1^2 (1 - \cos 2\pi f\tau) + P_2^2 (1 - \cos 4\pi f\tau)}{P_1^2 \sin 2\pi f\tau + P_2^2 \sin 4\pi f\tau} = - \frac{R_{nl}}{I_{nl}} \quad (26)$$

RESULTS AND DISCUSSION

A. Parametric Study of Response Functions

A series of calculations were made, utilizing the previously described computer program, in order to determine the effect of a variety of boundary conditions on the magnitude of the response functions for evaporating liquid oxygen droplets. The thermodynamic properties used in the calculations were:

$$\text{Thermal diffusivity} = 7.56 \times 10^{-7} \text{ ft}^2/\text{sec}$$

$$\text{Liquid density} = 72 \text{ lbm/ft}^3$$

$$\text{Prandtl number} = .712$$

$$\text{Gas viscosity} = 4.2 \times 10^{-5} \text{ lbm/ft-sec}$$

$$\text{Vapor specific heat} = .288 \text{ BTU/lbm}^\circ\text{F}$$

$$\text{Liquid thermal conductivity} = 2.21 \times 10^{-5} \text{ BTU/ft-sec-}^\circ\text{F}$$

$$\text{Gas thermal conductivity} = 4.04 \times 10^{-5} \text{ BTU/ft-sec-}^\circ\text{F}$$

$$\text{Isentropic exponent} = 1.135$$

$$\text{Initial drop temperature} = 140^\circ\text{R}$$

$$\text{Combustion gas temperature} = 6500^\circ\text{R}$$

The vapor pressure and heat of vaporization of the liquid oxygen is evaluated as a function of the drop surface temperature by

$$p_v(\text{lb/ft}^2) = e^{16.93 - \frac{1476}{T - 3.57}}$$

$$\lambda(\text{BTU/lbm}) = 61.33 + .5916T - .00248T^2$$

The following parameters were varied over the range indicated:

Chamber pressure: 100-600 psia

Initial drop radius: 15-150 microns

Final gas velocity: 400-2400 ft/sec

Initial drop velocity: 50-200 ft/sec

Frequency of oscillation: 200-30,000 cps

Amplitude of fundamental (Δp_1): $.01p_c - .8p_c$

Amplitude of harmonic (Δp_2): $0 - 1.2 \Delta p_1$

Table I gives the full range of tests conducted with boundary conditions and response functions.

A cursory look at the values calculated for the in-phase nonlinear response factor, R_{nl} , indicates many values that are greater than those previously found by the methods of Refs. 2 and 4. The present study includes the effects of finite thermal conductivity which, as discussed previously, causes a significant decrease in the time required for the drop surface to reach an effective equilibrium temperature. In addition, the temperature of the drop center remains relatively unchanged over the entire lifetime of the drop with the temperature gradient in the drop concentrated at the drop outer surface. Both these factors make the drop more sensitive to fluctuations in ambient pressure and temperature with concomitant increased response factors.

The major cause of larger response factors obtained in this study, however, appears to be due primarily to the effect of wave distortion, i.e., inclusion of harmonics in the ambient pressure field. This causes more relative peaks and valleys in the impressed pressure oscillation with attendant increases in evaporation rate. Another significant contributing effect is the presence of the array of drops in a varying gas velocity field.

Figures 3 and 4 indicate the quantitative effect of wave distortion and amplitude on the nonlinear in-phase response factor, R_{nl} . For the case of a constant ratio of the first harmonic to fundamental wave pressure amplitude, $\Delta p_2/\Delta p_1=0.8$, Figure 3, the variation of R_{nl} is relatively independent of fundamental amplitude provided $\Delta p_1 \geq 0.1p_c$. For the case where the fundamental amplitude is small, $\Delta p_1=0.01p_c$, the response factor increases significantly to a maximum value of $R_{nl}=1.68$. This behavior agrees qualitatively with that shown in Figure 2 of NASA TN D-6287, Ref. 5. Figures 4a, 4b and 4c show the effect of variations in the relative magnitude of the harmonic amplitude. The maximum response curve occurs at a value of $\Delta p_2=0.8\Delta p_1$. This too is in agreement with the results found in Ref. 5. It is

observed from Figures 4a,b,c that the frequency at which the maximum value of R_{nl} occurs decreases with increasing fundamental amplitude.

Figure 4b contains the results of calculations made for zero harmonic content, $\Delta p_2=0$. As discussed above, the results obtained in Ref. 4, NASA TN D-3749, also were for the case of no harmonic content in the pressure oscillation. The magnitude of the response factors calculated in this study for $\Delta p_2=0$ are lower than those obtained with non-zero harmonics and are consistent with those obtained in NASA TN D-3749.

The final gas velocity greatly affects the value of R_{nl} . This effect is observed in Figure 5 at all frequencies. A crossplot was made at 1200 Hz, Figure 6, and the final gas velocity extended on the low scale to 50 feet per second with drop velocities of 100 feet per second. It is seen that the value of the nonlinear in-phase response factor increases to 2.36 at a final gas velocity of 200 feet per second. It is also observed that the values of R_{nl} are about twice those observed in the previous Figures 3 and 4. In the regime $\Delta p_1 \geq 0.1 p_c$, the values and behavior of the nonlinear response factor, R_{nl} , agree both qualitatively and quantitatively with those shown in Figure 7, NASA TN D-6287, Ref. 5.

An attempt was made to correlate all of the response factor data obtained utilizing the transformed frequency suggested in Refs. 2 and 4. However, the buckshot nature of the resulting curves indicated that while qualitative agreement between the two studies is obtained, the previous correlations are unsuitable for the kind of model employed in this study. In order to correlate the data it was necessary to use a transformed response factor together with a modified transformed frequency. The transformations were obtained by trial and error in an attempt to minimize the data scatter. It was found that rather than include the effects of wave amplitude and distortion in the transformed coordinates, the effect of these variables could best be seen by utilizing parametric curves.

The transformed frequency is defined as

$$F = f \left(\frac{1200}{u_f} \right)^{1/3} \left(\frac{300}{p_c} \right)^{1/3} \left(\frac{r}{50} \right)^{3/2}$$

and the transformed response factor is

$$R_{n\ell} \left(\frac{u_f}{1200} \right)^{.56} \left(\frac{100}{v_D} \right)^{.15} \left(\frac{300}{p_c} \right)^{.1} \left(\frac{50}{r} \right)^{.12}$$

Figure 7 shows the results of the correlation study with separate curves to depict the effect of wave distortion and amplitude. For fundamental amplitudes greater than $.1p_c$ the effect of fundamental amplitude is not significant, but the effect of harmonic amplitude must be considered. Decreasing the fundamental amplitude to $0.01p_c$ causes significant increases in the response factor.

The study was extended to include the correlation of the in-phase fundamental response factor R_1 and harmonic response factor R_2 , and these are shown in Figures 8 and 9. Both response factors are transformed similar to $R_{n\ell}$ and correlated against the transformed frequency factor cited above. The fundamental response factor increases with the amplitude of the harmonic and is relatively insensitive to variations in the amplitude of the fundamental for $\Delta p_1 \geq .1p_c$. The magnitude of the harmonic response function increases with a decrease in the magnitude of the harmonic pressure oscillation component. Response factors, R_2 , on the order of 3.0 were calculated for harmonic amplitudes equal to 0.2 times the fundamental amplitude. The qualitative behavior, and the juxtaposition of these curves, agree with those shown in Figure 8, Ref. 5. The curves shown in Figures 7, 8, 9 represent the best fit through the available data. Deviations from the curve were generally less than 10% from the curve.

Figures 10, 11 and 12 represent the correlation of the results for the nonlinear out-of-phase response factor, $I_{n\ell}$, the fundamental

out-of-phase response factor, I_1 , and the harmonic out-of-phase response factor, I_2 . The I_{nl} curves were correlated with transformations similar to those employed for the in-phase response factor. The shape of the curve is similar to a cubic with a relative maximum point in the transformed frequency range of 300-400 cps and a relative minimum at a frequency corresponding to the location of the maximum point on the R_{nl} curves.

The results for the correlation of the out-of-phase fundamental response factor indicate that wave amplitude and distortion have no effect. In addition, excellent correlation was obtained by transforming I_1 by a multiple of $(300/p_c)^{.1}$ and the frequency by a multiple of $(r/50)^{3/2}$. Thus the final gas velocity and initial drop velocity are not effective in varying the magnitude of I_1 .

The correlation of the data for the out-of-phase harmonic response factor, I_2 , required utilizing a transformed ordinate

$$I_2 \left(\frac{u_f}{1200} \right)^{.2} \left(\frac{100}{v_D} \right)^{.15} \left(\frac{300}{p_c} \right)^{.1}$$

plotted against a transformed frequency

$$f \left(\frac{r}{50} \right)^{3/2}$$

Correlation also required the use of parametric curves to display the effect of wave distortion; i.e., the magnitude of I_2 decreases with increasing harmonic component amplitude.

In Figure 13, a correlation of a Princeton type "n" was plotted vs. frequency factor, F . It is seen to remain essentially constant over a broad spectrum of frequency factor. The value of "n" increases with the amplitude of the harmonic pressure perturbation amplitude.

Figure 14 is a plot of τ vs. frequency of oscillation for a variety of drop radii, initial drop velocity, final gas velocity and amplitude of pressure disturbance. The variation of the values of

of the parameters cited above are those which normally occur in liquid rocket engine practice. The results indicate that it is possible to correlate the values of τ with the frequency of oscillation without any significant dependence on any of the other parameters. The correlation seems to indicate a relationship between τ and f of the form,

$$f\tau = \text{constant}.$$

The value of τ is determined from Eq. (26). The right-hand side of the equation, i.e., $R_{n\ell}/I_{n\ell}$, has a value in the range 0.1 to 4.0 for the vast majority of cases tested in this study. The corresponding values for $2\pi f\tau$ are in the range 250 to 350 degrees. These, when plotted for the specific case tested, yielded essentially a straight line on a log-log plot as is suggested in the above equation.

The data from the above studies were regrouped for each of the seven response factors to show the effects of fundamental pressure perturbation amplitude (Δp_1), harmonic pressure perturbation amplitude (Δp_2), injection velocity (V_D), final gas velocity (u_f), droplet radius (r) and chamber pressure (P_c). The following table shows a summary of the relative effects of the various parameters on the different response factors:

	Δp_1	Δp_2	V_D	u_f	R	P_c
$R_{n\ell}$	weak	moderate	weak	strong	strong	weak
R_1	weak	strong	weak	strong	strong	moderate
R_2	weak	strong	weak	strong	strong	weak
$I_{n\ell}$	weak	moderate	weak	moderate	moderate	weak
I_1	weak	weak	weak	weak	moderate	weak
I_2	weak	moderate	moderate	moderate	moderate	weak
n	weak	strong	moderate	strong	moderate	weak
τ	independent of all parameters					

B. Effect of Thermal Conductivity

In general, it was found that the nonlinear in-phase response factor, R_{nl} , was not very sensitive to variations of up to 10^3 in the liquid thermal conductivity, for the frequency range of interest in combustion instability studies. These results are explained below.

The calculation for the R_{nl} requires the summation of the instantaneous evaporation rate of the complete array of drops in the chamber over an interval of time. Thus, any particular local event resulting from the interaction of the pressure wave and one drop is masked by the summation of all the other events occurring at the same time. In other words, the random event associated with each drop is masked by the stochastic behavior of the drop array.

A second reason for the insensitivity of R_{nl} to the thermal conductivity variation is that an open loop analysis is assumed. There is no feedback to the wave behavior from the droplet evaporation. This feedback can be significant in deforming the wave shape, and consequently the response factor, R_{nl} . The wave shape can be deformed not only by coupling the relaxation time to the evaporation but also by the amount of vaporization occurring from the array of drops during the coupling. These two situations are discussed below for a particular case.

The drop is introduced at a uniform temperature of 140°R . The drop surface heats up to about 240°R and remains at that temperature during its lifetime. For a 50μ radius oxygen drop, and normal thermal conductivity, it takes 1.99×10^{-6} sec. for the drop surface to reach 238°R . For the drop with high thermal conductivity, i.e., 10^{-2} Btu $\text{ft}^{-1}\text{R}^{-1}\text{sec}^{-1}$, it takes 1.87×10^{-4} sec. for the drop surface to reach 239°R . It is noticed that the time lag differs by about two orders of magnitude. In a closed loop analysis, this difference in time lag could mean the difference in the effective coupling of the drop evaporation to drive the passing pressure wave.

For the case where the normal thermal conductivity is employed, the drop center does not appreciably heat up during its lifetime. For example, after 90% of the drop mass has evaporated, the temperature of the drop center is still 144°R. As found previously (Ref. 3), the temperature gradient is concentrated at the drop outer surface. For the case where the large thermal conductivity is used, it is found that the drop remains uniform in temperature. The uniform temperature drop has a much larger thermal inertia than the normal drop; thus the dynamic behavior of these drops would be very different, not only in the lag times, but also in the mass evaporation response to a disturbance. For example, for a passing compression wave, the normal drop would obtain a much greater surface temperature than the uniform temperature drop for the same amount of heat transfer to the droplet. If one includes the nonlinearity of the Clausius-Clapeyron equation, then the additional mass evaporation in the former case would be much greater, with increased concomitant response factor.

SUMMARY OF RESULTS

The objective of this investigation was to analytically determine stability parameters relating drop vaporization response rates in a liquid rocket combustor to nonlinear-high amplitude pressure oscillations for drops vaporizing with finite liquid thermal conductivity. The results of the program can be summarized as follows:

1. A computer program was developed for determining the vaporization response of droplets with finite thermal conductivity to high amplitude distorted pressure oscillations.
2. Drop vaporization responses for an array of drops traveling through a rocket combustor are significantly different than the response of a single drop stationary in a flow field.
3. The vaporization rate responses were very dependent on drop size, final gas velocity in the combustor and wave distortion. The responses were moderately dependent on liquid droplet velocity and weakly dependent on chamber pressure and wave amplitude.

4. A general correlation scheme was developed to relate various response numbers that can be used in stability analyses to combustor operating conditions.

5. For the Princeton type time lag response, the time lag was found to be inversely proportional to the frequency, resulting in a phase lag of 250 to 350 degrees.

REFERENCES

1. Priem, R.J. and Heidmann, M.F.: "Propellant Vaporization as a Design Criteria for Rocket-Engine Combustion Chambers". NASA TR R-67, 1960.
2. Heidmann, M.F. and Wieber, P.R.: "Analysis of n-Heptane Vaporization in Unstable Combustors with Travelling Transverse Oscillations". NASA TN D-3424, 1966.
3. Agosta, V.D. and Hammer, S.S.: "Droplet Vaporization with Liquid Heat Conduction". Propulsion Sciences, Inc., NASA CR-72672, 1970.
4. Heidmann, M.F. and Wieber, P.R.: "Analysis of Frequency Response Characteristics of Propellant Vaporization". NASA TN D-3749, 1966.
5. Heidmann, M.F.: "Amplification by Wave Distortion of the Dynamic Response of Vaporization Limited Combustion". NASA TN D-6287, 1971.
6. Private communication with R.J. Priem.
7. Heidmann, M.F.: "Frequency Response of a Vaporization Process to Distorted Acoustic Disturbances". NASA TN D-6806, 1972.

TABLE I

* PARAMETRIC STUDY OF RESPONSE FUNCTIONS

* Unless otherwise noted, the boundary conditions used to calculate the response functions are:

Chamber pressure $p_c = 300$ psia

Drop radius = 50 microns

Drop initial temperature = 140°R

Drop initial velocity = 100 ft/sec

Final gas velocity = 1200 ft/sec

Amplitude of fundamental pressure perturbation; $\Delta p_1 = .2 p_c$

Amplitude of harmonic pressure perturbation; $\Delta p_2 = .8 \Delta p_1$

f	R_{nl}	R_1	R_2	I_{nl}	I_1	I_2	n	$\tau \times 10^3$
150	.289	.244	.359	.345	.252	.491	.404	5.7
200	.351	.276	.468	.442	.389	.524	.519	4.3
400	.581	.526	.666	.448	.606	.20	.541	2.019
800	.810	.910	.654	.185	.265	.0603	.538	.873
1500	.986	1.112	.789	.232	.216	.025	.65	.46
3000	.941	1.04	.781	.255	.193	.352	.682	.24
6000	.831	.987	.628	.44	.355	.583	.63	.125
12000	.549	.8	.255	.684	.609	.802	.73	.071
30000	.086	.340	-.309	.765	.808	.967	.4	.032

$\Delta p_1 = .1 p_c$

600	.674	.720	.602	.425	.558	.216	.555	1.3
1200	.911	.854	1.0	.131	.189	.0415	.606	.56
2400	1.026	1.032	.823	.241	.162	.411	.632	.316
5000	.844	.979	.635	.412	.329	.542	.627	.152
10000	.623	.843	.275	.630	.547	.760	.729	.084

f	R_{nl}	R_1	R_2	I_{nl}	I_1	I_2	n	$\tau \times 10^3$
<u>$\Delta P_1 = .4 P_c$</u>								
250	.431	.316	.612	.438	.466	.394	.525	3.35
500	.724	.783	.631	.331	.503	.061	.527	1.507
1200	.891	.998	.725	.160	.214	.071	.590	.57
3000	.920	1.012	.757	.240	.182	.338	.615	.236
8000	.742	.916	.470	.518	.423	.666	.647	.099
<u>$\Delta P_1 = .8 P_c$</u>								
400	.683	.672	.7	.322	.485	.067	.501	1.89
800	.948	1.091	.724	-.001	.003	-.0072	.674	.84
1600	.941	.979	.882	.115	.0625	.197	.628	.41
2500	.918	.995	.797	.196	.152	.265	.609	.277
6000	.814	.938	.621	.387	.299	.526	.599	.126
<u>$\Delta P_2 = 0 \quad \Delta P_1 = .2 P_c$</u>								
800	.566	.566	-	.075	.075	-	.3	.67
1500	.692	.692	-	.096	.096	-	.305	.331
3000	.488	.488	-	.176	.176	-	.273	.202
6000	.43	.43	-	.32	.32	-	.335	.117
12000	.244	.244	-	.54	.54	-	.673	.072
<u>$\Delta P_2 = .2 \quad \Delta P_1$</u>								
800	.791	.656	3.16	.102	.137	.322	.418	.68
1600	.874	.722	3.61	.185	.176	.399	.470	.36
3000	.72	.635	3.16	.188	.209	.580	.400	.196
6000	.655	.566	2.95	.346	.315	.792	.430	.111
12000	.455	.432	2.5	.530	.525	1.11	.550	.067

f	R_{nl}	R_1	R_2	I_{nl}	I_1	I_2	n	$\tau \times 10^3$
<u>$\Delta P_2 = 1.2 \quad \Delta P_1$</u>								
400	.548	.618	.499	.334	.716	.068	.427	2.03
800	.689	1.04	.445	.130	.295	.015	.500	.448
1500	.87	1.30	.574	.250	.193	.264	.557	.27
3000	.831	1.33	.587	.362	.302	.403	.538	.254
6000	.698	1.23	.408	.461	.371	.509	.583	.133
12000	.380	.984	.098	.710	.627	.755	.941	.076

<u>$\Delta P_2 = .2 \quad \Delta P_1 \quad \Delta P_1 = .1 \quad P_c$</u>								
600	.642	.551	2.91	.411	.352	.191	.470	1.155
1500	.873	.743	4.135	.280	.291	-.005	.500	.404
4000	.821	.725	3.195	.151	.156	.472	.441	.140
10000	.519	.441	2.475	.536	.516	.665	.557	.077

<u>$\Delta P_2 = 1.2 \quad \Delta P_1 \quad \Delta P_1 = .1 \quad P_c$</u>								
600	.580	.788	.435	.302	.630	.075	.422	1.327
1200	.773	1.067	.568	.205	.300	.139	.644	.325
2500	.956	1.532	.62	.33	.060	.437	.719	.317
5000	.749	1.23	.410	.388	.131	.494	.544	.159
10000	.475	1.051	-.091	.664	.696	.732	.780	.088

<u>$\Delta P_2 = 1.2 \quad \Delta P_1 \quad \Delta P_1 = .8 \quad P_c$</u>								
400	.631	.774	.531	.034	.538	.029	.418	1.93
1000	.922	1.146	.513	.110	-.2	.128	.486	.557
2500	.831	1.098	.575	.174	-.214	.216	.487	.255
6000	.720	1.12	.539	.415	.167	.496	.512	.134

<u>$\Delta P_2 = .2 \quad \Delta P_1 \quad \Delta P_1 = .8 \quad P_c$</u>								
400	.558	.498	2.06	.385	.378	.557	.428	1.76
800	.798	.722	2.69	-.041	.0752	.229	.420	.603
1600	.774	.688	2.99	+.032	-.0429	.100	.368	.322

f	R_{nl}	R_1	R_2	I_{nl}	I_1	I_2	n	$\tau \times 10^3$
2500	.784	.671	2.52	.098	-.0166	.119	.379	.217
6000	.688	.61	2.27	.2926	.0934	.632	.360	.106

$\Delta P_2 = .8$	ΔP_1	$\Delta P_1 = .2$	P_c	$U_g = 400$				
300	1.43	1.636	1.112	.848	1.130	.403	1.147	2.6
600	1.950	2.22	1.510	.3177	.3677	.239	1.290	1.13
1000	2.082	2.50	1.429	.090	.344	.463	1.380	.68
2000	1.720	2.12	1.340	.182	.0805	.366	1.166	.329
4000	1.645	1.941	1.181	.353	.262	.496	1.095	.1755
9000	1.390	1.755	.821	.616	.502	.786	1.007	.0834

$U_g = 2400$								
400	.414	.322	.557	.416	.466	.326	.476	2.09
800	.608	.636	.563	.260	.391	.056	.435	.935
2000	.699	.743	.630	.086	.1	.062	.466	.332
5000	.693	.776	.562	.383	.330	.466	.537	.152
12000	.425	.603	.147	.595	.518	.715	.719	.076

$U_g = 400 \quad V_D = 50$								
300	1.11	1.185	.994	.715	.977	.304	.926	2.62
600	1.533	1.750	1.196	.162	.262	.0056	1.028	1.098
1500	1.724	1.933	1.397	.147	.126	.180	1.164	.434
4000	1.551	1.8	1.164	.231	.178	.315	1.029	.168
9000	1.298	1.63	.766	.587	.487	.743	.941	.0836

$U_g = 2400 \quad V_D = 50$								
400	.398	.313	.531	.430	.440	.347	.465	2.09
800	.599	.623	.561	.244	.390	.0179	.424	.929
2000	.679	.663	.575	.035	.066	-.0133	.431	.319
5000	.652	.724	.539	.359	.318	.422	.505	.154
12000	.406	.578	.138	.591	.518	.703	.724	.073

f	$R_{n\ell}$	R_1	R_2	$I_{n\ell}$	I_1	I_2	n	$\tau \times 10^3$
<u>$U_g=400 \quad V_D=200$</u>								
600	2.415	2.876	1.694	.254	.246	.266	1.619	1.097
1000	2.00	2.59	1.064	.145	.075	.255	1.355	.648
2000	1.805	2.036	1.438	-.026	-.047	.0057	1.275	.191
4000	1.707	1.96	1.35	.135	.06	.253	1.155	.168
9000	1.5	1.86	.937	.515	.382	.723	1.03	.0809

<u>$U_g=2400 \quad V_D=200$</u>								
800	.716	.868	.478	.374	.402	.332	.544	.958
2000	.779	.939	.528	.237	.101	.451	.527	.359
5000	.700	.758	.610	.339	.2811	.430	.518	.152
12000	.442	.633	.148	.601	.523	.721	.718	.072

<u>$U_g=1200 \quad V_D=200$</u>								
200	.441	.331	.612	.499	.459	.564	.578	4.25
800	1.056	1.087	1.008	.209	.308	.0557	.7	.862
1500	1.22	1.44	.867	.1482	.519	.425	.858	.494
3000	1.019	1.2	.735	.288	.131	.535	.685	.237
6000	.935	1.101	.675	.425	.334	.567	.679	.125
12000	.586	.85	.173	.695	.621	.816	.810	.071

<u>$U_g=1200 \quad V_D=50$</u>								
200	.321	.253	.426	.416	.354	.511	.494	4.32
800	.733	.82	.596	.161	.223	.0646	.486	.87
1500	.825	.889	.724	.084	.113	.037	.554	.44
3000	.923	1.004	.795	.323	.305	.350	.635	.243
6000	.79	.928	.574	.452	.384	.557	.622	.129
12000	.508	.738	.149	.667	.597	.777	.791	.072

f	$R_{n\ell}$	R_1	R_2	$I_{n\ell}$	I_1	I_2	n	$\tau \times 10^3$
<u>r=15μ $U_g=1200$ $V_D=100$</u>								
2000	.431	.340	.573	.473	.507	.428	.551	.423
4000	.660	.713	.577	.374	.409	.162	.518	.193
7000	.792	.822	.745	.197	.225	.153	.528	.1
15000	.811	.914	.627	.474	.18	.538	.641	.05
30000	.578	.781	.261	.600	.325	.719	.695	.028
<u>r=150μ</u>								
150	.888	.990	.730	.168	.259	.0266	.589	4.58
300	1.111	1.25	.913	.299	.17	.228	.747	2.31
600	1.052	1.217	.793	.462	.297	.563	.758	1.25
1200	.822	1.029	.497	.575	.501	.691	.718	.664
3000	.261	.565	-.233	.740	.718	.665	1.342	.311
<u>r=50μ $p_c=100$</u>								
500	.712	.797	.580	.195	.258	.096	.477	1.42
1000	.853	.967	.676	.162	.172	.147	.565	.687
2000	.870	.953	.741	.191	.165	.232	.577	.348
4000	.783	.897	.603	.281	.211	.390	.541	.183
8000	.629	.799	.362	.523	.429	.669	.620	.102
<u>$p_c=600$</u>								
500	.568	.498	.677	.501	.637	.296	.587	1.65
1000	.847	.959	.672	.255	.348	.109	.572	.718
2000	1.05	1.167	.866	.3	.285	.325	.706	.357
4000	.974	1.105	.769	.343	.262	.469	.671	.183
8000	.803	1.00	.493	.567	.475	.711	.706	.099
16000	.401	.711	-.083	.792	.760	.842	1.119	.056

Symbols

a	speed of sound
A_d	droplet surface area
C_D	drag coefficient
C_{pv}	droplet vapor specific heat
D	molecular diffusion coefficient
f	frequency
h	film heat transfer coefficient
k	liquid thermal conductivity
k_m	vapor-gas mixture thermal conductivity
K_g	mass transfer coefficient
M	molecular weight
m	droplet mass
p_c	mean chamber pressure
P_v	vapor pressure
Δp_1	amplitude of fundamental pressure perturbation
Δp_2	amplitude of harmonic pressure perturbation
r	droplet radius
\dot{r}_s	regression rate of droplet surface
Re	Reynolds number
t	time
T_c	chamber temperature
T_s	droplet surface temperature
U	gas velocity
V_d	drop velocity
\dot{w}	mass evaporation rate
α	thermal diffusivity
γ	isentropic exponent
ρ	density
λ	heat of vaporization
μ	viscosity

APPENDIX B

Calculation Procedure and Program Listing

The procedure used in calculating the droplet evaporation histories, temperature distribution within the drop and response factors is illustrated by the flow diagram.

Step 1. Load into the machine the following boundary conditions, initial conditions and computational parameters.

Card 1. (14 I5) NRUN - Number of test case
 NMONTH - Month
 MDAY - Day
 MYEAR - Year
 JA - Number of calculation steps between
 output for each drop
 NA - Number of mesh points minus one within
 drop
 NP - Number of drops injected per cycle
 NY - Number of summation histories per period
 NART - Number of artificial drops insisted
 between each of the NP calculated drops

Card 2. (8E 10.4) S - Initial drop radius (ft.)
 PO - Mean chamber pressure (lbf/ft²)
 VGAF - Final gas velocity (ft/sec)
 VDI - Initial drop velocity (ft/sec)
 DPC - Ratio of peak-to-peak fundamental pressure
 oscillation to mean chamber pressure
 DPCI - Ratio of harmonic pressure oscillation
 to fundamental oscillations
 OMEGA - Frequency of pressure oscillations (cps)
 A - Stretching parameter (1.3)

Card 3. (8E 10.4)

STAB	- Initial time increment (sec.)
TFO	- Mean combustion gas temperature ($^{\circ}\text{R}$)
TO	- Initial droplet temperature ($^{\circ}\text{R}$)
THETA	- Phase angle of pressure oscillation
AJ_0	- Zero order Bessel function $J_0\left(\frac{1.841\text{R}}{\text{Rw}}\right)$
AJ_1	- First order Bessel function $J_1\left(\frac{1.841\text{R}}{\text{Rw}}\right)$
AJ_2	- Second order Bessel function $J_2\left(\frac{1.841\text{R}}{\text{Rw}}\right)$
RWR	- Ratio of radial location in chamber to wall radius

Card 4. (8E 10.4)

GAMMA	- Ratio of specific heats for combustion gases
ALPHA	- Liquid thermal diffusivity (ft^2/sec)
RHOL	- Liquid density (lbm/ft^3)
RR	- Universal gas constant
PCA	- Critical pressure - droplet (lb/ft^2)
PCB	- Critical pressure - combustion gases (lb/ft^2)
TCA	- Critical temperature - droplet ($^{\circ}\text{R}$)
TCB	- Critical temperature - combustion gases ($^{\circ}\text{R}$)

Card 5. (8E 10.4)

EMA	- Molecular weight - droplet
EMB	- Molecular weight - gases
AA	- Constant in diffusivity equation - 2.33×10^{-6}
BB	- Constant in diffusivity equation - 1.823
EMV	- Molecular weight of drop vapor
PR	- Prandtl number of gases
AKB	- Combustion gas thermal conductivity ($\text{BTU}/\text{ft}\cdot\text{sec}\cdot^{\circ}\text{R}$)
CPV	- Drop vapor specific heat

Card 6. (8E 10.4)

VIS	- Combustion gas viscosity ($\text{lbm}/\text{ft}\cdot\text{sec}$)
AK	- Drop thermal conductivity ($\text{BTU}/\text{ft}\cdot\text{sec}\cdot^{\circ}\text{R}$)

Step 2. Write out the value of all input variables and calculate all parameters that are constant throughout calculations. Initialize droplet and gas parameters to begin calculation of N^{th} drop history. Redefine variables as follows:

$$U = Tr \quad (A1)$$

so that Eq. (7) becomes

$$U_t = \alpha U_{tt} \quad (A2)$$

The space variable within the drop is also redefined:

$$a = r/s \quad (A3)$$

where s is the drop surface radius as a function of time.

The space variable is further redefined as:

$$X = A\sigma(z+1/(A-z)) - \sigma \quad (A4)$$

wh

where

$$\sigma = (A-1)/(A^2+1-A) \quad (A5)$$

and A is a stretching parameter which concentrates mesh points near the surface of the drop. The heat conduction equation (A2) can now be written:

$$U_T = \left(\frac{\alpha S_t z Y}{s} + \alpha Y Y_x / s^2 \right) U_x + \frac{\alpha Y^2}{s^2} U_{xx} \quad (A6)$$

where $Y = \frac{dx}{dz}$.

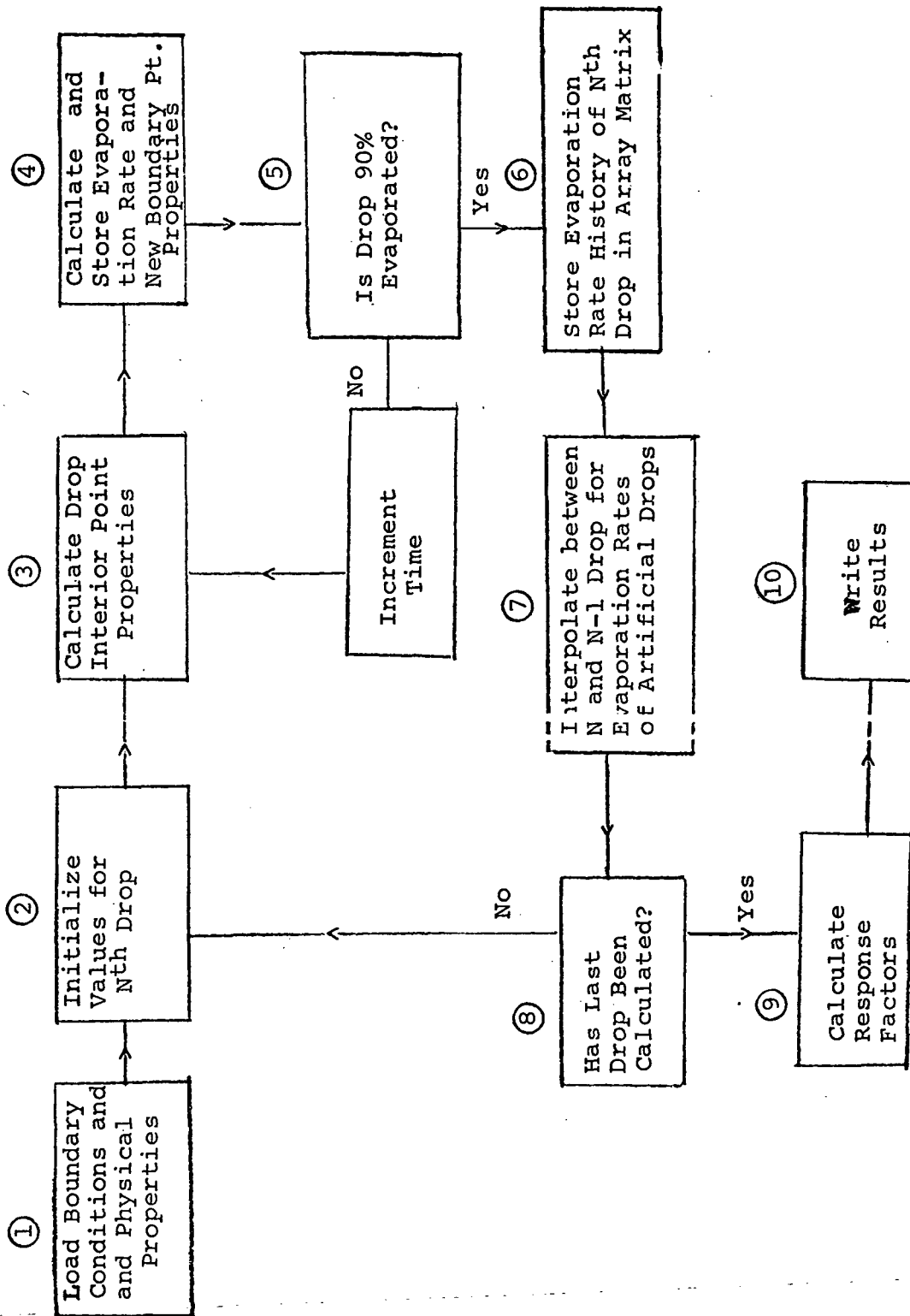
Step 3. The interior point calculations are performed (temperature distribution within the drop) by utilizing a finite difference scheme for the solution of the transformed heat conduction equation based upon the current values of drop surface temperature and heat transfer rate to the drop.

Step 4. Droplet evaporation rates, changes in combustion gas properties, droplet velocity and net heat transfer to the drop are calculated by solving Eqs. (10) through (17). The evaporation rate is stored for future summation

in the array history. Intermediate results are printed at the end of every JA time increments.

- Step 5. If the drop is not 90% evaporated, time and other thermodynamic and dynamic variables are incremented and control is transferred to Step 3.
- Step 6. If the drop has reduced to 10% of its initial mass, the evaporation rate is transferred into the array summation matrix at a predetermined number of points during the period (NY).
- Step 7. An interpolation of the evaporate rate between the N^{th} and $(N-1)^{\text{th}}$ drop is made for each of the artificial drops injected between two drops for which calculations are performed. These evaporation rates are added to the array matrix.
- Step 8. Test for end of evaporation calculations.
- Step 9. Calculation of response factors by solving Eqs. (18) through (26).
- Step 10. Print results.

The machine computation time is primarily a function of the number of drops injected per cycle. For the case described in Figs. 1 and 2, i.e., eight drops injected per cycle, a total of 160 seconds of CDC 6600 computer time was required.



FLOW CHART

```

PROGRAM DROPS(INPUT,OUTPUT,TAPE5 = INPUT,TAPE6 = OUTPUT)
C
C PROGRAM DROPS WITH RNL,INL,R1,R2,I1,I2,F,G, AND N AND TAU AUG. 7
C
000003 COMMON WWW(3000),TTT(3000),W(400),INDEX,KK2,VEL,VD,AKG,DD,PPV,H,D
000003 1M1,SIT,S,TIME,J,K,JA,NA,NC,DX,DT,ST,SN,STN,WDOT,P,TF
000003 COMMON SAVW(30,400),MARK,KK,NART,NN,NP
000003 COMMON X(64),Z(64),AB(64),AC(64),AD(64),UO(64),U(64),UN(64),T(64)
1R(64)
C
000003 PV(W) = 2980.9579867*EXP(8.928-1476.5/(W-3.568))
000016 SL(W) = 61.33+.5916*W-.00248*W**2
000025 D(W,0) = DD1/W*AA*(O/DD2)**BB
C
C NA=NUMBER OF MESH POINTS MINUS ONE
C JA=NUMBER OF STEPS BETWEEN OUTPUTS FOR THE FIRST DROP
C NP=NUMBER OF DROPS INJECTED PER CYCLE
C NY=NUMBER OF SUMMATION HISTORIES PER PERIOD (400 MAXIMUM)
C A=STRETCHING PARAMETER
C
000036 READ(5,250) NRUN,MONTH,MDAY,MYEAR,JA,NA,NP,NY,NART
000064 READ(5,260) S,P0,VGAF,VDI,DPC,DPC1,OMEGA,A
000110 READ(5,260) STAB,TF0,T0,THETA,AJ0,AJ1,AJ2,RWR
000134 READ(5,260) GAMMA,ALPHA,RHOL,RR,PCA,PCB,TCA,TCB
000160 READ(5,260) EMA,EMB,AA,BB,EMV,PR,AKB,CPV
000204 READ(5,260) VIS,AK
000214 DD2 = SQRT(TCA*TCB)
000221 DD1 = (PCA*PCB)**.333333/SQRT(EMA*EMB/(EMA+EMB))*(TCA*TCB)**.4166
17
000241 TAV = (TF0+T0)*.5
000244 ROAV = P0*EMB/(RR*TAV)
000247 SCH = VIS/ROAV/U(PU,IAV)
000253 SIT = S
000254 NC = NA+1
000256 TAU = 1./OMEGA
000260 NX = NY-1
000262 DTST = TAU/FLOAT(NX)
000264 DTBAR = TAU/FLOAT(NP)
000266 WRITE(6,320)
000271 WRITE(6,330)NP,NART,NY
000303 WRITE(6,270)NRUN,MONTH,MDAY,MYEAR,JA,P0,TF0,S,T0,VGAF,VDI
000335 WRITE(6,340) OMEGA,THETA,DPC,AJ0,AJ1,AJ2,RWR
000357 WRITE(6,280) ALPHA,RHOL,RR,PCA,PCB,TCA,TCB,EMA,EMB,EMV,AA,BB,SCH
1PR,AKB,CPV,AK,GAMMA,VIS
000431 WRITE(6,290)
000435 WRITE(6,300) NA,A,STAB
000447 WRITE(6,410)DPC1
C
C CONVERT DPC TO 1/2 PEAK TO PEAK PERTURBATION
C
C CONVERT DPC1 TO RATIO OF DPI TO P0
C
000455 DPC=DPC/2.
000457 DPC1=DPC*DPC1
000460 PI = 4.*ATAN(1.)
000464 DUMB=PI*4.*RHOL
000466 PI2 = 2.*PI

```

```

000467      PI02 = PI/2.
000471      POMEGA = PI2*OMEGA
000473      GA = (GAMMA-1.)/GAMMA
000475      VD = VDI
000477      TI = 0.
000500      CC1=DPC*(AJ0-AJ2)*.430/GAMMA
000504      CC2=RWR*AJ1*.467*DPC/GAMMA
000510      DUM4 = EMV/2./RR
000513      DX = 1./FLOAT(NA)
000515      DDX = 1./DX
000516      DDX2 = 1./DX/DX
000520      TWODX=2.*DX
000521      SIG = (A-1.)/(A*(A-1.)+1.)
000526      A1 = A*SIG
000527      A2 = 2.*A1
000530      A3 = SIG*(A**2+1.)
000533      A4 = A2**2/SIG
000534      DO 1 I=1,30
000536      DO 1 J=1,400
000537      1 SAVW(I,J)=0.

C
C      INITIALIZATION OF VALUES FOR THE (NN)TH DROP
C
000547      DO 220 NN = 1,NP
000550      S = SIT
000552      S2 = S**2
000553      SN = S
000554      WDOT = 0.
000555      STS = 0.
000556      ST = 0.
000557      K = 0
000560      J = 0
000561      DT = STAB
000562      TIME = DTBAR*(NN-1)
000566      KK1 = 0
000567      KK2 = 0
000570      VD = VDI
000571      P=P0*(1.+.859*DPC*AJ1*COS(POMEGA*TIME-THETA)+.859*DPC1*AJ1*COS(2.
1POMEGA*TIME))
000613      TF = TF0*(P/P0)**GA
000620      TAV = (TF0+T0)*.5
000623      ROAV = P0*EMB/(RR*TAV)
000626      SCH = VIS/ROAV/D(P*TAV)
000632      DUM2 = .6*PR**.333333
000636      DO 10 N = 1,NC
000637      X(N) = DX*FLOAT(N-1)
000642      Z(N) = (A3+X(N)-SQRT((A3+X(N))**2-A4*X(N)))/A2
000656      R(N) = Z(N)*S
000660      F = X(N)/A1+1./A-Z(N)
000665      F2 = F*F
000666      F3 = F*F2
000667      Y = A1*(1.+F2)
000672      AR(N) = Z(N)*Y
000675      AC(N) = A2*F3*ALPHA
000700      T(N) = T0
000701      IF (N.EQ.NA) YNA = Y
000704      AD(N) = Y**2*ALPHA
000707      U(N) = R(N)*T0

```

```

000711      10 CONTINUE
000712      TINT = TIME
C
C      TIME DEPENDENT COMPUTATION BEGINS HERE
C
000715      20 IF(NN.EQ.1.AND.J.EQ.JA)CALL OUTPUT
000726          K = K+1
000730          J = J+1
000731          IF(K.LT.100) GO TO 40
000733          DT=STAB*10.
000735          IF(K.LT.200) GO TO 40
000737          DT = 100.
000741          DO 30 N = 1,NA
000742              DT3 = (R(N+1)-R(N))*2/ALPHA/4.
000746              IF (DT.LT.DT3) GO TO 30
000751              DT = DT3
000751      30 CONTINUE
000754      40 TIME = TIME+DT
000756          UN(1) = 0.
C
C      INTERIOR POINT COMPUTATION BEGINS HERE
C
000757          LOOP = 0
000760      50 DO 70 N = 2,NA
000762              NQ = N+LOOP
000764              NM = NQ-1
000766              UX = (U(NQ)-U(NM))*DDX
000771              UXX = (U(N+1)+U(N-1)-2.*U(N))*DDX2
000776              AE = AB(N)*STS+AC(N)/S2
001002              AG = AD(N)/S2
001004              UT = AE*UX+AG*UXX
001007              IF (LOOP.EQ.1) GO TO 60
001011              UN(N) = U(N)+UT*DT
001015              GO TO 70
001016      60 UN(N) = (UO(N)+U(N)+UT*DT)*.5
001024      70 CONTINUE
C
C      BOUNDARY POINT COMPUTATION BEGINS HERE
C
001027          DT1 = DT
001030          TIM = 0.
001031          TI = TIME-DT
001032          KIM=30
001033          DT1 = DT/FLOAT(KIM)
001035      80 CONTINUE
001035          IF (LOOP.EQ.0) SN = S+ST*DT
001041          IF (LOOP.EQ.1) SN = .5*(S+S0+ST*DT)
001050          TNAMN = UN(NA-1)/SN/Z(NA-1)
001053          IF (LOOP.EQ.0) GO TO 90
001054          T(NC) = UO(NC)/S0
001057          U(NC) = UO(NC)
001060          S = S0
001061      90 TI=TIME-DT/2.
001064          P=P0*(1+.859*DPC*AJ1*COS(POMEGA*TI-THETA)+.859*DPC1*AJ1*COS(2.*P/
            1MEGA*TI))
001106          TF = TF0*(P/P0)**GA
001113          TAV = (TF+T(NC))*5
001116          DD = D(P,TAV)

```

```

001120      ROAV = P*EMB/(RR*TAV)
001123      VOR = VIS/ROAV
001125      DUM1 = .6*(VOR/DD)**.333333
001132      AS = SQRT(GAMMA*32.2*P/ROAV)
001140      VR=CC1*AS*(COS(POMEGA*TI+PID2-THETA)+DPC1/DPC*COS(2.*POMEGA*TI+PII
12))
001161      VH=CC2*AS*(COS(POMEGA*TI-THETA)+DPC1/DPC*COS(2.*POMEGA*TI))
001200      VGA = VGAF*(1.-(S/SIT)**3)
001204      DV = VGA-VD
001206      VT = 5.65*(ROAV*ABS(DV))**.16*(VIS/S)**.84*DV/RHOL/S
001224      VD=VD+VT*DT/2.
001230      VEL=SQRT(DV**2+VR**2+VH**2)
001237      DOM1 = SQRT(2.*VEL*S/VOR)
001244      H = AKR/2./S*(2.+DUM2*DOM1)
001251      AKG = (2.+DUM1*DOM1)*DD*DUM4/S/TAV
001257      AKGP=AKG*P
001261      S1=S
001262      95 PPV=PV(T(NC))
001266      DUM=1.-PPV/P
001271      IF (DUM.GT.1.E-20) GO TO 100
001274      WRITE (6,310)
001277      CALL OUTPUT
001300      CALL EXIT
001301      100 DUM=AKGP*ALOG(DUM)
001305      STN = DUM/RHOL
001307      DUM = -DUM
001310      TR = -((T(NC)-TF)*H-(T(NC)-TF0)*DUM*CPV+DUM*SL(T(NC)))/AK
001325      TNAM = T(NA-1)+(TNAMN-T(NA-1))*TIM/DT
001332      TX=(T(NC)-TNAM)/TWODX
001336      SIM =S1+ST*DT1
001341      RNA= S1*Z(NA)
001343      TRNA = TX*YNA/S1
001345      TRR = (TR-TRNA)/(S1-RNA)
001351      UR = T(NC)+S)*TR
001355      UT = ALPHA*(S1*TRR+2.*TR)+UR*ST
001363      UN(NC) = U(NC)+UT*DT1
001367      T(NC) = UN(NC)/SIM
001371      ST = STN
001372      S1= SIM
001373      TIM = TIM+DT1
001375      IF(TIM.LT.DT)GO TO 95
001377      IF (KIM.GT.0) SN = SIM
001402      DO 110 N = 1,NC
001404      UO(N) = U(N)
001406      R(N) = SN*Z(N)
001410      IF (N.NE.1) T(N) = UN(N)/R(N)
001414      110 U(N) = UN(N)
001420      SO = S
001422      S = SN
001423      S2 = S**2
001424      ST = STN
001425      STS = ST/S
001426      IF (LOOP.EQ.1) GO TO 120
001430      LOOP = 1
001431      GO TO 50
001432      120 CONTINUE

```

C

C

INTERIOR POINT CALCULATION AND BOUNDARY POINT CALCULATION END HERE

```

C
001432      WDOT = DUM8*S2*ST
001435      KK1 = KK1+1
001436      IF (KK1.LT.3) GO TO 130
001440      KK2 = KK2+1
001441      KK1 = 0
001442      WWW(KK2) = -WDOT
001444      TTT(KK2) = TIME
001445      130 CONTINUE
001445      T(1)=(UN(2)*Z(3)**2/Z(2)-UN(3)*Z(2)**2/Z(3))/(Z(3)**2-Z(2)**2)/SN
001456      IF (NN.EQ.1) GO TO 140
001460      RATIO = (S/SIT)**3
001463      IF (RATIO .GE. 0.1 ) GO TO 20
001465      TB=TIME-TINT
001467      WRITE (6,350) NN,RATIO
001477      GO TO 150
001500      140 IF (S.GT.0.4641589*SIT) GO TO 20
001505      WRITE (6,360)
001510      TB = TIME
001512      IF (NN.EQ.1) T90 = TB
001515      150 CONTINUE

C
C      COMPUTATION OF SUMMATION HISTORIES BEGINS HERE
C
001515      DUMA1=TB+DTBAR*(NN-1)
001523      DUMA2=TAU+DTBAR*(NN-1)
001527      IF(TB.GE.TAU)GO TO 155
001531      MARK=1
001532      DO 153 KK=1,NY
001533      IF(NN.EQ.1)W(KK)=0.
001536      TK=TB+(KK-1)*DTST
001543      IF(TK.GT.DUMA1.AND.TK.LT.DUMA2)TK=-100.
001554      IF(TK.GT.TB+DUMA2)TK=-100.
001560      IF(TK.GE.DUMA2)TK=TK-TAU
001565      INDEX=KK2
001567      W(KK)=FWDOT(TK)+W(KK)
001574      153 CONTINUE
001577      GO TO 220
001577      155 DO 210 KK=1,NY
001601      MARK=1
001602      TK = TB+(KK-1)*DTST
001607      I = 1
001610      160 T1 = TB+(I-1)*DTBAR
001616      IF (TK.GT.T1) GO TO 170
001621      II = I
001622      GO TO 180
001622      170 I = I+1
001624      GO TO 160
001624      180 CONTINUE
001624      IF (NN.EQ.1) W(KK) = 0.
001630      INDEX = KK2
001632      DO 190 N = 1,2
001633      IF (NN.LT.II.AND.N.EQ.1) GO TO 190
001642      JJ = N-1
001643      TI = TK-JJ*TAU
001646      W(KK) = W(KK)+FWDOT(TI)
001653      MARK=MARK+1
001654      190 CONTINUE

```

```

001656      NT = TK/TAU
001661      DO 200 NI = 2,NT
001663      T2 = NI*TAU*(NN-1)*DTBAR
001671      IF (TK.LT.T2) GO TO 200
001674      TI = TK-NI*TAU
001677      W(KK) = W(KK)+FWDOT(TI)
001704      MARK=MARK+1
001705 200 CONTINUE
001710 210 CONTINUE
001712 220 CONTINUE
001715      WRITE (6,380)
001720      WRITE (6,370) (W(KK),KK = 1,NY)
001733      WAV = 0.
001734      DO 230 KK = 1,NX
001736 230 WAV = WAV+(W(KK)+W(KK+1))/2.*DTST
001746      WAV = WAV/TAU
001747      WRITE (6,390) WAV

```

C
C
C

COMPUTATION OF RESPONSE FACTORS BEGINS HERE

```

001755      PSQ=0.
001756      P1SQ=0.
001757      P2SQ=0.
001760      PISQ=0.
001761      PI1SQ=0.
001762      PI2SQ=0.
001763      RNL=0.
001764      R1=0.
001765      R2=0.
001766      AINL=0.
001767      A11=0.
001770      A12=0.
001771      DO 231 KK=1,NY
001772      TK=TB+(KK-1)*DTST
001777      PM=1.
002001      IF (KK.EQ.1.OR.KK.EQ.NY) PM=.5
002011      APSQ=.859*AJ1*(DPC*COS(POMEGA*TK-THETA)+DPC1*COS(2.*POMEGA*TK))
002030      AP1SQ=.859*AJ1*DPC*COS(POMEGA*TK-THETA)
002040      AP2SQ=.859*AJ1*DPC1*COS(2.*POMEGA*TK)
002050      APISQ=.859*AJ1*(DPC*SIN(POMEGA*TK-THETA)+DPC1*SIN(2.*POMEGA*TK))
002067      AP11SQ=.859*AJ1*DPC*SIN(POMEGA*TK-THETA)
002077      AP12SQ=.859*AJ1*DPC1*SIN(2.*POMEGA*TK)
002107      WPRM=(W(KK)-WAV)/WAV
002112      RNL=RNL+PM*WPRM*APSQ
002115      R1=R1+PM*WPRM*AP1SQ
002120      R2=R2+PM*WPRM*AP2SQ
002123      AINL=AINL+PM*WPRM*APISQ
002126      A11=A11+PM*WPRM*AP11SQ
002131      A12=A12+PM*WPRM*AP12SQ
002134      PSQ=PSQ+PM*APSQ**2
002137      P1SQ=P1SQ+PM*AP1SQ**2
002143      P2SQ=P2SQ+PM*AP2SQ**2
002147      PISQ=PISQ+PM*APISQ**2
002153      PI1SQ=PI1SQ+PM*AP11SQ**2
002157 231 PI2SQ=PI2SQ+PM*AP12SQ**2
002166      RNL=RNL/PSQ
002167      R1=R1/P1SQ
002171      R2=R2/P2SQ

```



```

002172      AINL=AINL/PI SQ
002174      AI1=AI1/PI1 SQ
002175      AI2=AI2/PI2 SQ
002177      CAPF=OMEGA*(SIT/.000166)**1.5*(800./VGAF)**.3333*(.1/DPC)**.3333*
1(43200./P0)**.3333
002225      CAPG=CAPF*(VGAF/800.)*(7./3.)*(DPC/.1)**.633
002243      WRITE(6,400)RNL, R1,R2,AINL,AI1,AI2,CAPF,CAPG,T90

C
C          CALCULATION OF N AND TAU BEGINS HERE
C

002270      AP=.859*AJ1*DPC
002273      BP=.859*AJ1*DPC1
002275      WT=PI2/2000.
002277      SAVFX=0.
002300      SAVJ=0.
002301      DO 240 I=1,2000
002302      FX=RNL/AINL*(AP**2*SIN(WT)+BP**2*SIN(2.*WT))+BP**2*(1.-COS(2.*WT))
1+AP**2*(1.-COS(WT))
002335      IF (FX) 232,238,233
002336      232 J=-1
002337      GO TO 234
002340      233 J=1
002341      234 IF (J+SAVJ) 239,238,239
002344      238 WTS=WT+PI2/2000.*(FX/(SAVFX-FX))
002352      PTAU=WTS/POMEGA
002354      ANGLE=WTS*360./PI2
002356      PEN=RNL*(AP**2+BP**2)/(AP**2*(1.-COS(WT))+BP**2*(1.-COS(2.*WT)))
002377      WRITE(6,500) WTS,ANGLE,PTAU,PEN
002413      239 WT=(I+1)/2000.*PI2
002420      SAVFX=FX
002421      240 SAVJ=J
002425      CALL EXIT

C

002426      250 FORMAT (14I5)
002426      260 FORMAT (8E10.4)
002426      270 FORMAT (1H0, 10HRUN NUMBER15,5X,2HON13,1H/12,1H/12//
1          13H OUTPUT EVERY16,6H STEPS//14H GAS
2 PRESSURE=E13.5,7H LB/FT2/17H GAS TEMPERATURE=E13.5,8H RANKINE/24H
3 DROPLET INITIAL RADIUS=E13.5,3H FT/21H DROPLET TEMPERATURE=E13.5,
48H RANKINE/11H FINAL VGA=E13.5,7H FT/SEC/18H DROPLET VELOCITY=E13.
55,7H FT/SEC/51H AUTOMATIC STOP WHEN 90 PERCENT MASS HAS EVAPORATED
6)
002426      280 FORMAT (9H0 ALPHA,7X,4HRHOL,6X,12HGAS CONSTANT,3X,3HPCA,9X,3HPCF
1,9X,3HTCA,9X,3HTCB/7E12.4//4X,2HMA,10X,2HMB,10X,2HMV,11X,1HA,11X,1
2R,9X,3HSCH,9X,2HPR/7E12.4//4X,2HKB,8X,5H(CP)V,7X,5HKAPPA,7X,5HGAMA
3A,7X,3HVIS/5E12.4/)
002426      290 FORMAT (35H PV(T)=EXP(16.928-1476.5/(T-3.568))/36H LAMBDA(T)=61.33
1+.5916*T-.00248*T**2/83H D(P,T)=(PCA*PCB)**1/3/SQRT(MA*MB/(MA+MB))
2*(TCA*TCB)**5/12/P*A*(T/SQRT(TCA*TCB))**B)
002426      300 FORMAT (36HONUMBER OF INTERVALS INSIDE DROPLET=I3,23H, STRETCHING
1PARAMETER=E12.4/21H STABILITY PARAMETER=E12.4)
002426      310 FORMAT (6HOFALL1)
002426      320 FORMAT(1H1, 36HPROGRAM DROPS AUGUST 1972 VERSION )
002426      330 FORMAT(46H THE NUMBER OF CALCULATED DROPS PER PERIOD IS 15/58H THE
1 NUMBER OF ARTIFICIAL DROPS BETWEEN EACH REAL DROP IS 15/51H THE E
2VAPORATION FROM THE ENTIRE ARRAY IS SUMMED AT,14,18H POINTS PER PE
3RIOD)
002426      340 FORMAT(9H0 OMEGA,7X,5HTHETA,5X,10HDPC PK-PK,6X,3HAJ0,9X,3HAJ1,

```

```

19X,3HAJ2,9X,3HRWR/7E12.4)
002426 350 FORMAT(1H0,5HDROP IS,36H CALCULATION ENDS WITH A MASS RATIO=E10.3)
002426 360 FORMAT (1H0,5X,32H90 PERCENT EVAPORATION COMPLETED)
002426 370 FORMAT (1X,10E10.3)
002426 380 FORMAT (1H1,6H W IS)
002426 390 FORMAT(1X,5H WAV= E12.5)
002426 400 FORMAT(1X,5H RNL= E12.5/1X,5H R1= E12.5/1X,5H R2= E12.5/1X,5H INL=
1 E12.5/1X,5H I1= E12.5/1X,5H I2= E12.5/1X,5H F = E12.5/1X,5H G =
2E12.5/1X,5H T90=E12.5, 8H SECONDS)
002426 410 FORMAT(1X,5HDPC1=E12.5,5X,9H(DP1/DPC) )
002426 500 FORMAT(/// 9H WTS = E12.5,8H RADIANS/9H ANGLE = E12.5,8H DEGREES
1/9H TAU = E12.5,8H SECONDS/9H N = E12.5)
002426 END

```

```

000003      FUNCTION FWDOT (T)
COMMON WWW(3000),TTT(3000),W(400),INDEX,KK2,VEL,VD,AKG,DD,PPV,H,DO
1M1,SIT,S,TIME,J,K,JA,NA,NC,DX,DT,ST,SN,STN,WDOT,P,TF
000003      COMMON SAVW(30,400),MARK,KK,NART,NN,NP
C
000003      IF(T.LT.TTT(1))FWDOT=0.
000006      IF(T.LT.TTT(1)) GO TO 30
000010      IF (T .GT.TTT(KK2)) FWDOT = WWW(KK2)
000015      IF(T.GT.TTT(KK2)) GO TO 30
000021      DO 10 I = 1,INDEX
000022      L = INDEX+1-I
000024      IF (TTT(L).GE.T ) GO TO 10
000027      LM = L
000030      GO TO 20
000031      10 CONTINUE
000034      20 LP = LM+1
000036      INDEX = LP
000037      EPS = (TTT(LM)-T )/(TTT(LM)-TTT(LP))
000044      FWDOT = WWW(LM)+EPS*(WWW(LP)-WWW(LM))
C
C      BEGINNING OF ARTIFICAL DROP CALCULATION
C
000051      30 IF(NART.EQ.0) RETURN
000054      WW=FWDOT
000056      DLAST=0.
000057      IF(NN.NE.1) GO TO 40
000061      SAVW(MARK,KK)=WW
000065      ART=0.
C
C      ADDS IN CONTRIBUTION FROM DROP 1 FOR INTERPOLATION WITH LAST DROP
C
000065      DO 35 I=1,NART
000067      35 ART=ART+FLOAT(I)/FLOAT(NART+1)*WW
000100      FWDOT=FWDOT+ART
000101      RETURN
000102      40 IF(NN.EQ.NP) DLAST=1.
000106      ART=0.
000107      DO 50 I=1,NART
000111      50 ART=ART+SAVW(MARK,KK)+FLOAT(I)/FLOAT(NART+1)*(WW-SAVW(MARK,KK))
1      +DLAST*(WW-FLOAT(I)/FLOAT(NART+1)*WW)
000136      SAVW(MARK,KK)=FWDOT
000142      FWDOT=FWDOT+ART
000143      RETURN
000144      END

```

```

SURROUTINE OUTPUT
000002 COMMON WWW(3000),TTT(3000),W(400),INDEX,KK2,VEL,VD,AKG,DD,PPV,H,NO
1M1,SIT,S,TIME,J,K,JA,NA,NC,DX,DT,ST,SN,STN,WDOT,P,TF
000002 COMMON SAVW(30,400),MARK,KK,NART,NN,NP
000002 COMMON X(64),Z(64),AB(64),AC(64),AD(64),UO(64),U(64),UN(64),T(64),
1R(64)

C
000002 DUM = TIME
000004 WRITE (6,40) K,DUM,SN,ST,WDOT
000021 NH = (NC+1)/2
000024 NM = NC/2
000025 DO 10 N = 1,NH
000027 L = NM+N
10 WRITE (6,30) N,R(N),T(N),L,R(L),T(L)
000053 IF (K.EQ.0) GO TO 20
000054 REY = DOM1**2
000055 DUM = (S/SIT)**3
000060 WRITE (6,50) H,REY,DUM,DT
000073 WRITE (6,70) VEL,VD,AKG,DD,PPV
000111 WRITE (6,60) P,TF
000121 20 CONTINUE
000121 J = 0
000122 RETURN

C
000123 30 FORMAT (I9,2E15.5(I9,2E15.5)
000123 40 FORMAT (1H0//5X,4HSTEP16,10X,5HTIME=E12.4,5X,3HRS=E12.4/24X,6HRSDO
1T=E12.4,5X,5HWDOT=E12.4//18X,1HR,13X,1HT,24X,1HR,13X,1HT)
000123 50 FORMAT (2X,2HH=E10.3,1X,4HREY=E10.3,1X,11HMASS RATIO=E10.3,1X,3HDT
1=E10.3)
000123 60 FORMAT (2X,2HP=E10.3,1X,3HTF=E10.3)
000123 70 FORMAT (2X,4HVEL=E10.3,3HVD=E10.3,4HAKG=E10.3,3HDD=E10.3,4HPPV=E10.
13)
000123 END

```

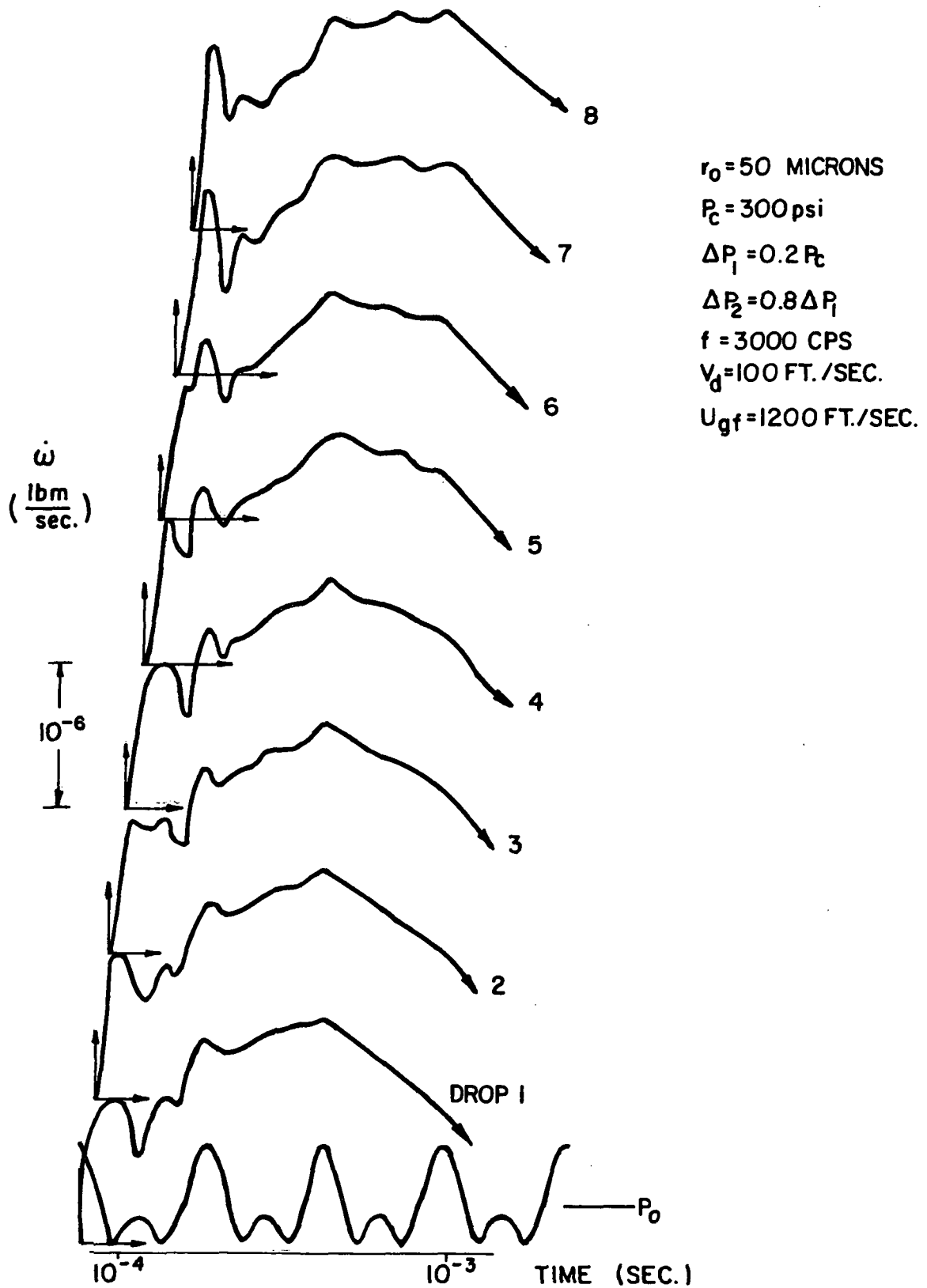


FIG. 1

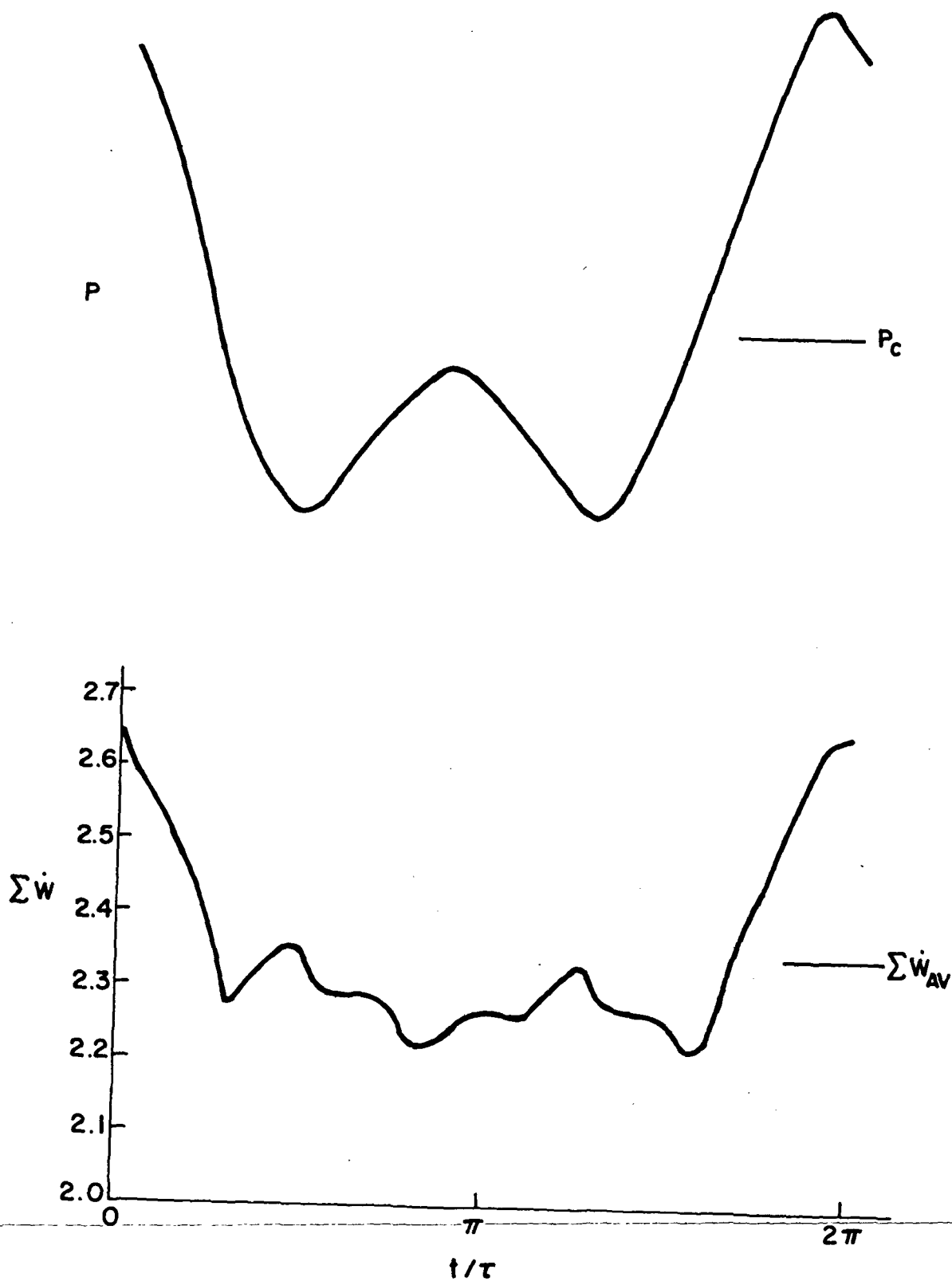


FIG.2 ARRAY EVAPORATION RATE VS. TIME

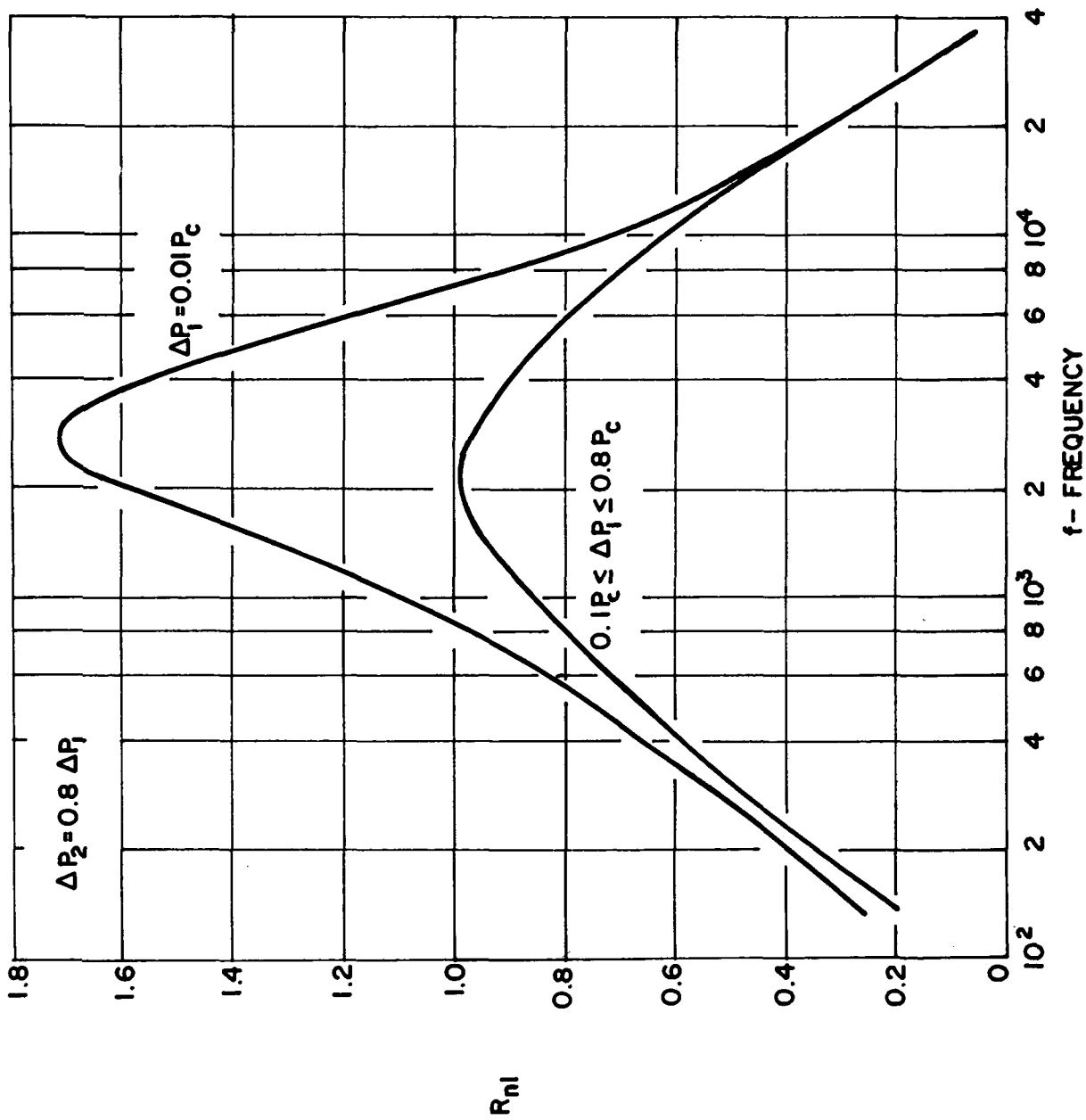


FIG. 3 RESPONSE FACTOR VS. FREQUENCY: EFFECT OF AMPLITUDE

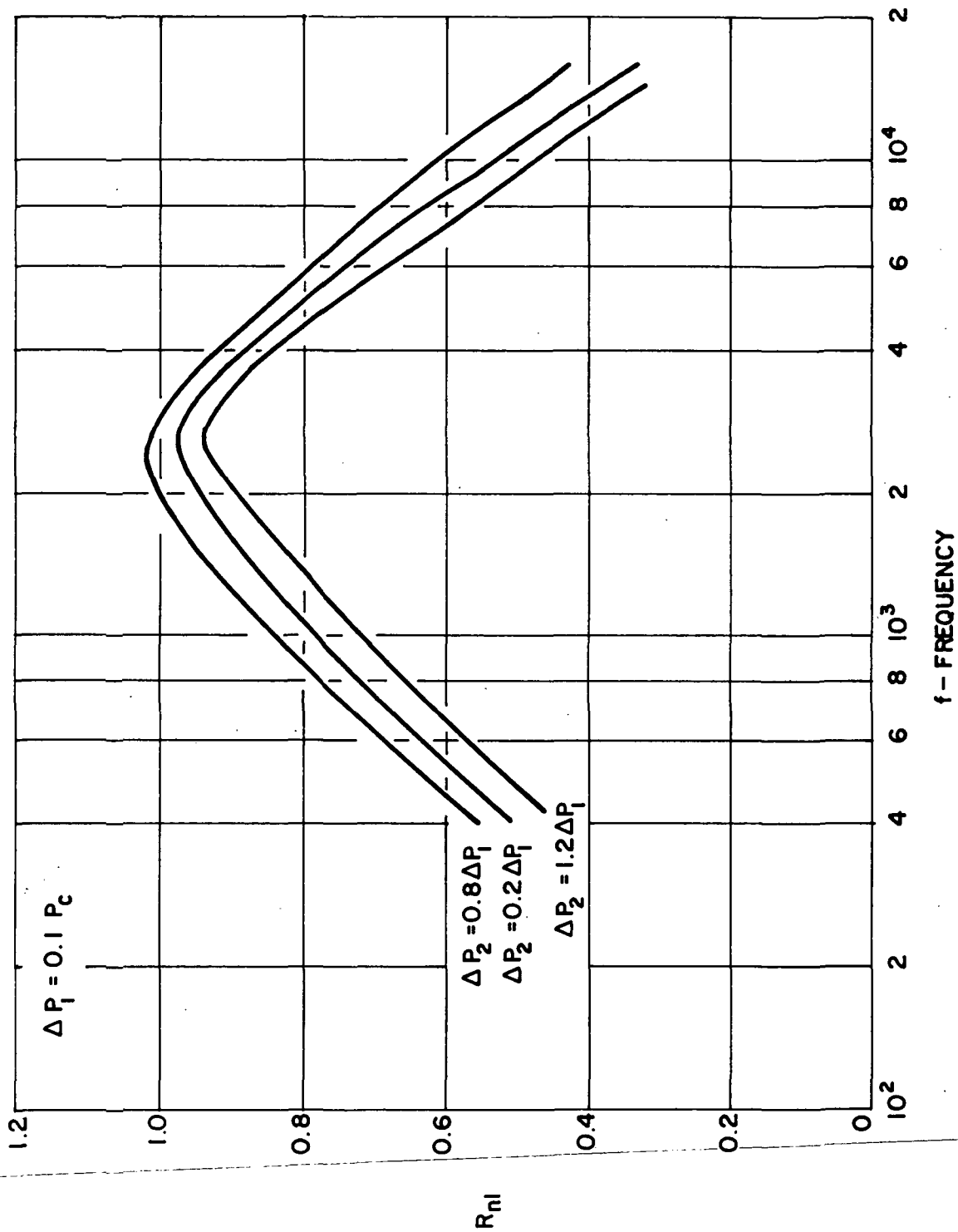


FIG. 4a RESPONSE FACTOR VS. FREQUENCY: EFFECT OF DISTORTION
 $\Delta P_1 = 0.1 P_c$

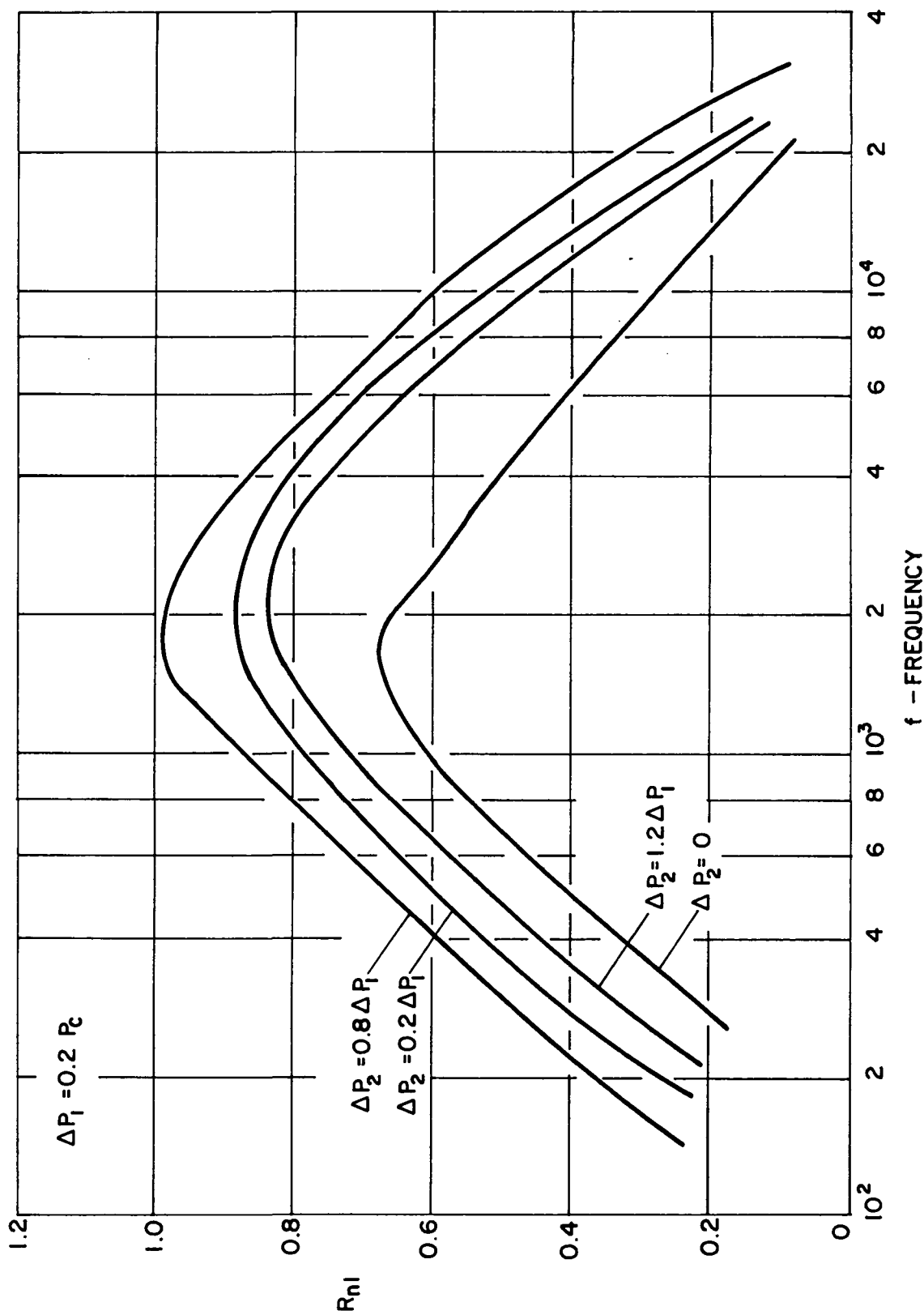


FIG. 4b RESPONSE FACTOR VS. FREQUENCY: EFFECT OF DISTORTION
 $\Delta P_1 = 0.2 P_c$

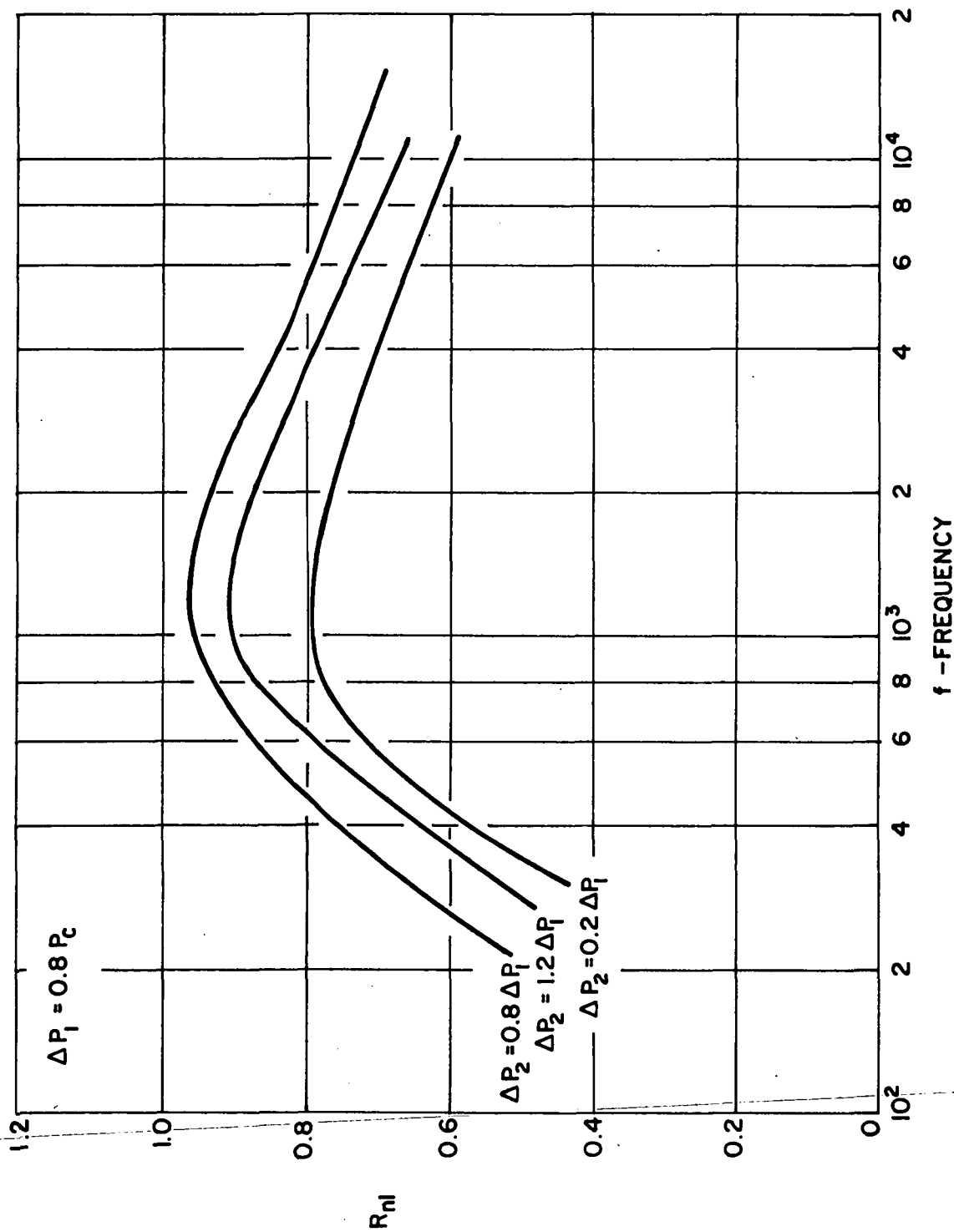


FIG. 4c RESPONSE FACTOR VS. FREQUENCY: EFFECT OF DISTORTION
 $\Delta P_1 = 0.8 P_c$

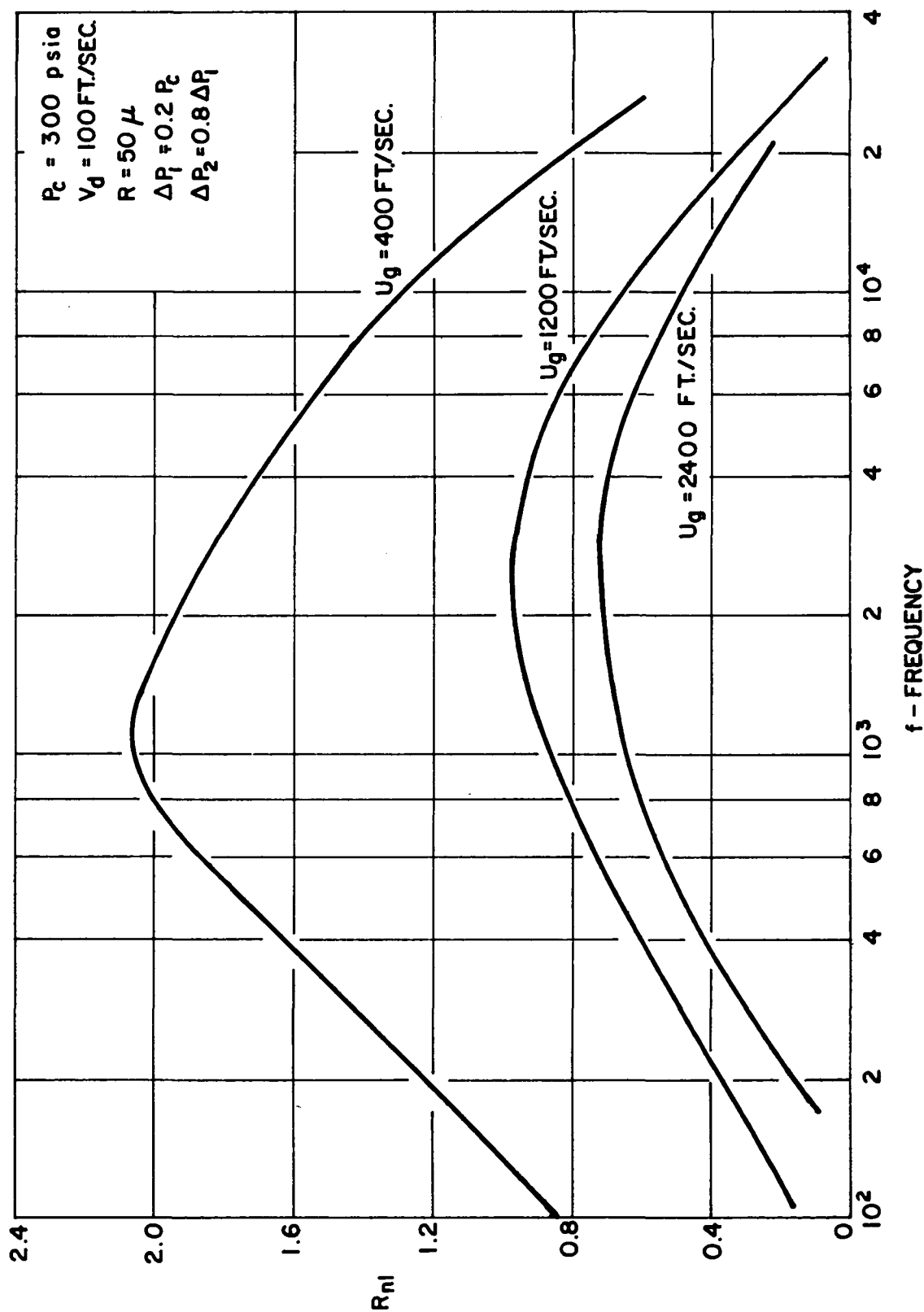


FIG. 5 RESPONSE FACTOR VS. FREQUENCY: EFFECT OF FINAL GAS VELOCITY

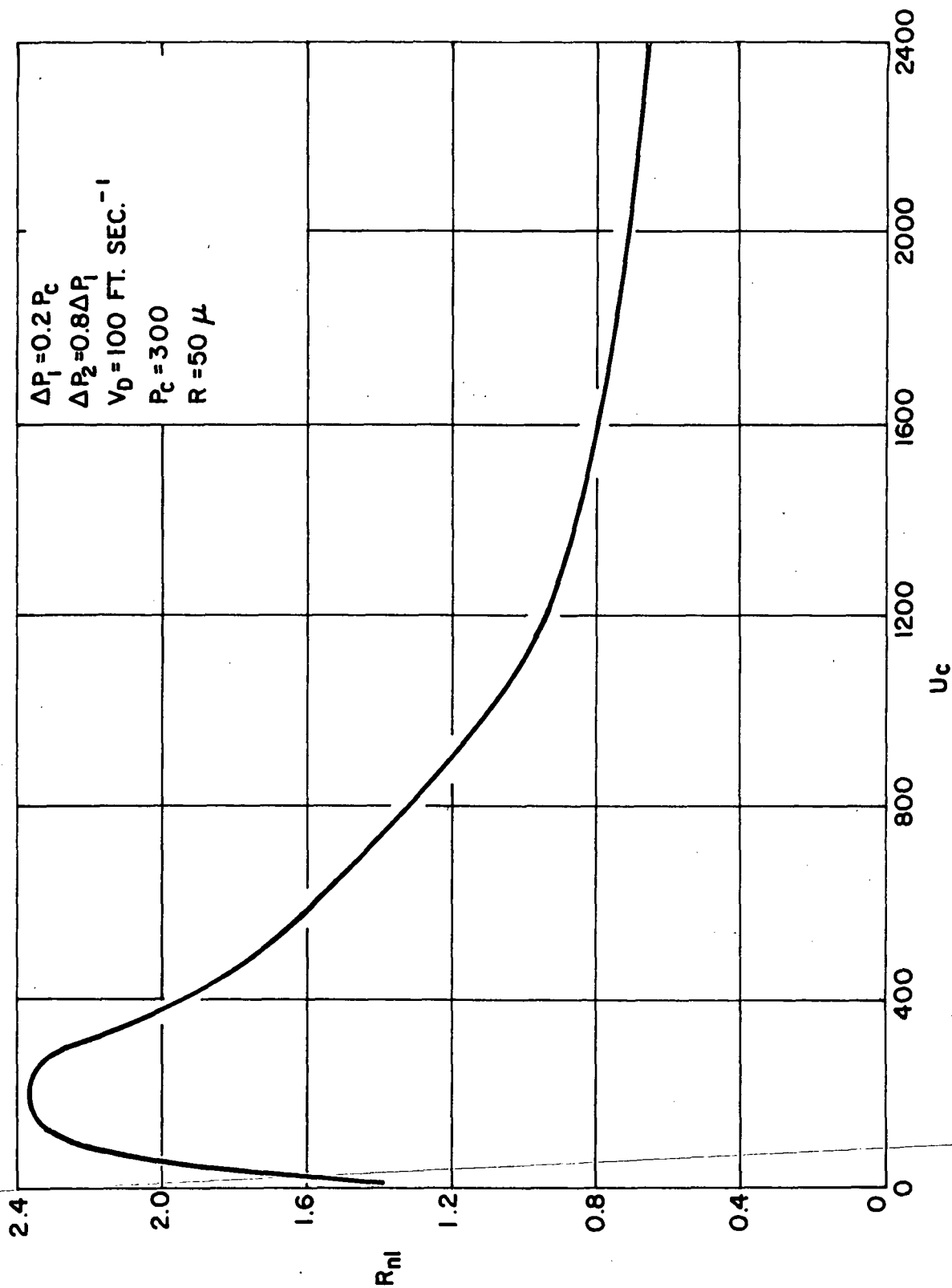


FIG. 6 RESPONSE FACTOR VS. FINAL GAS VELOCITY

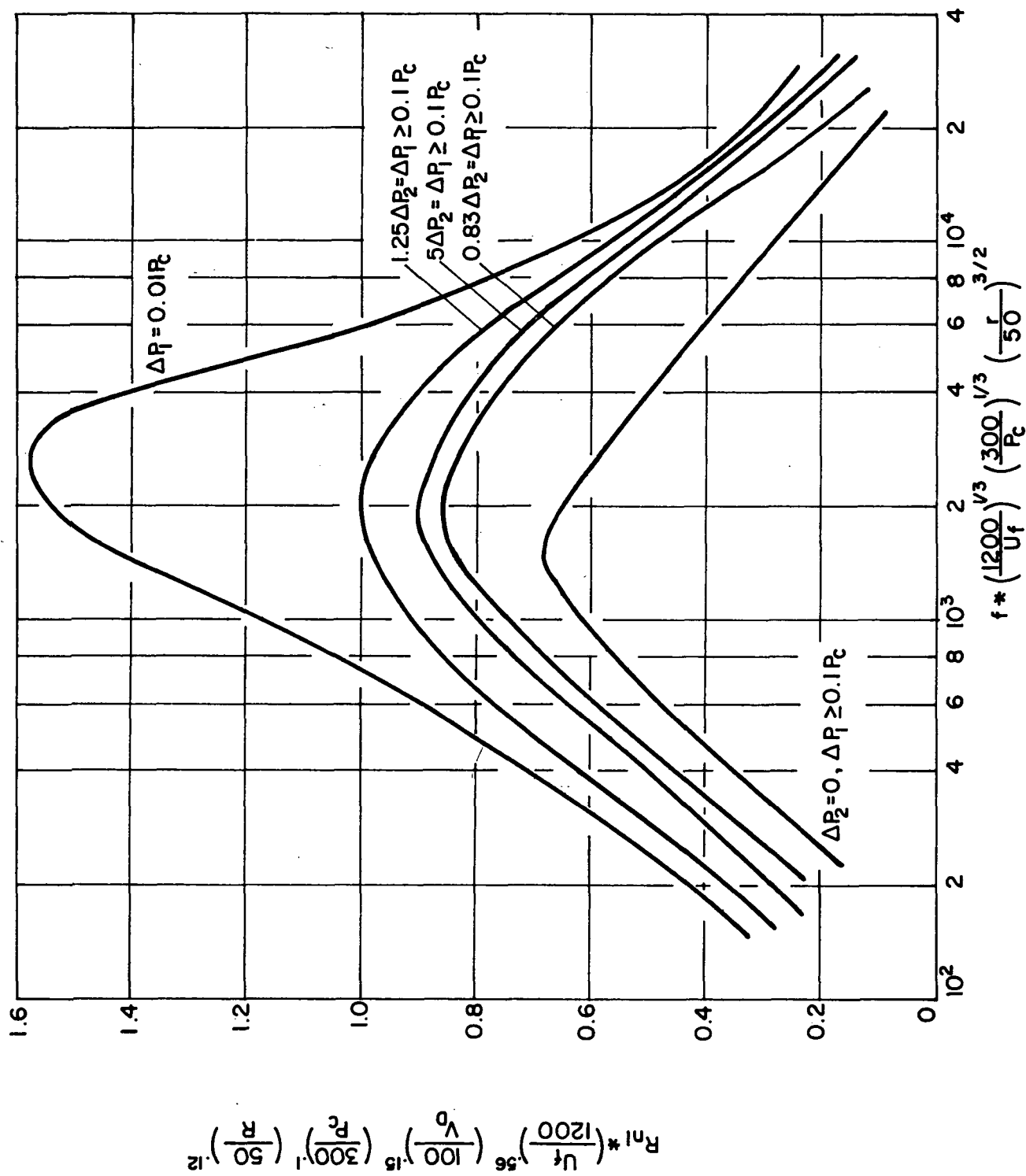


FIG.7 IN PHASE NON-LINEAR RESPONSE FACTOR VS. FREQUENCY FACTOR

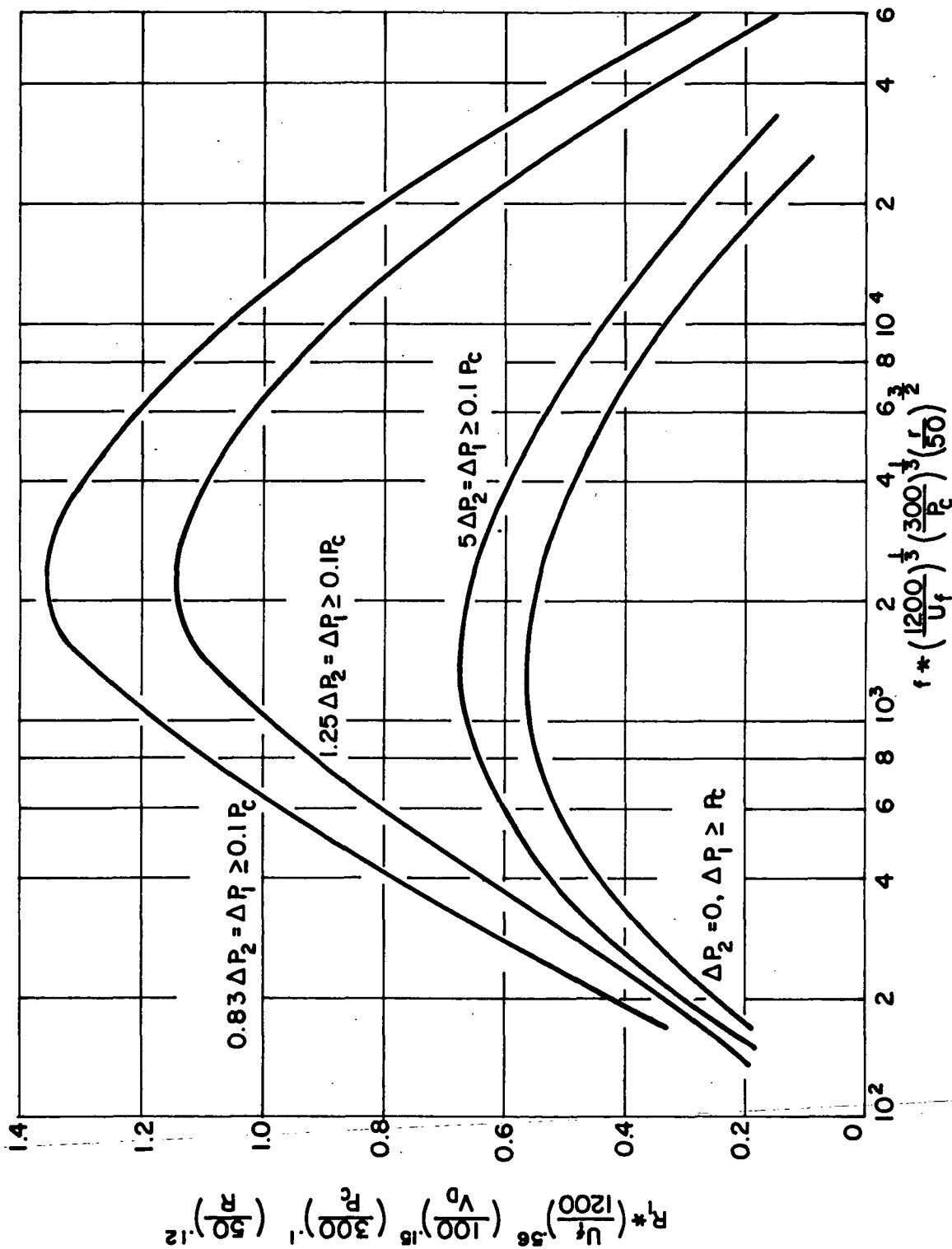


FIG. 8 IN PHASE FUNDAMENTAL RESPONSE FACTOR VS. FREQUENCY FACTOR

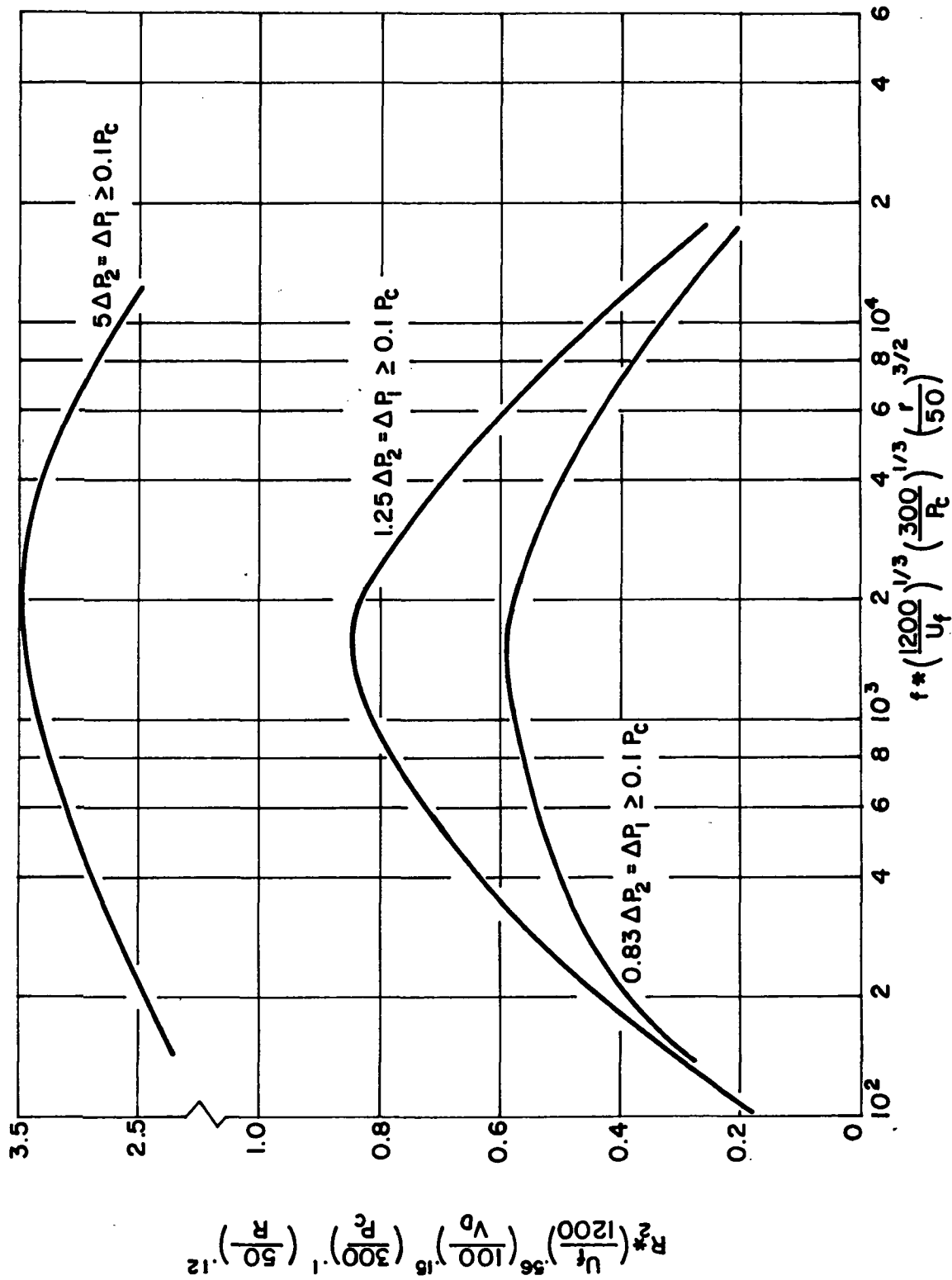


FIG.9 FIRST HARMONIC RESPONSE FACTOR VS. FREQUENCY FACTOR

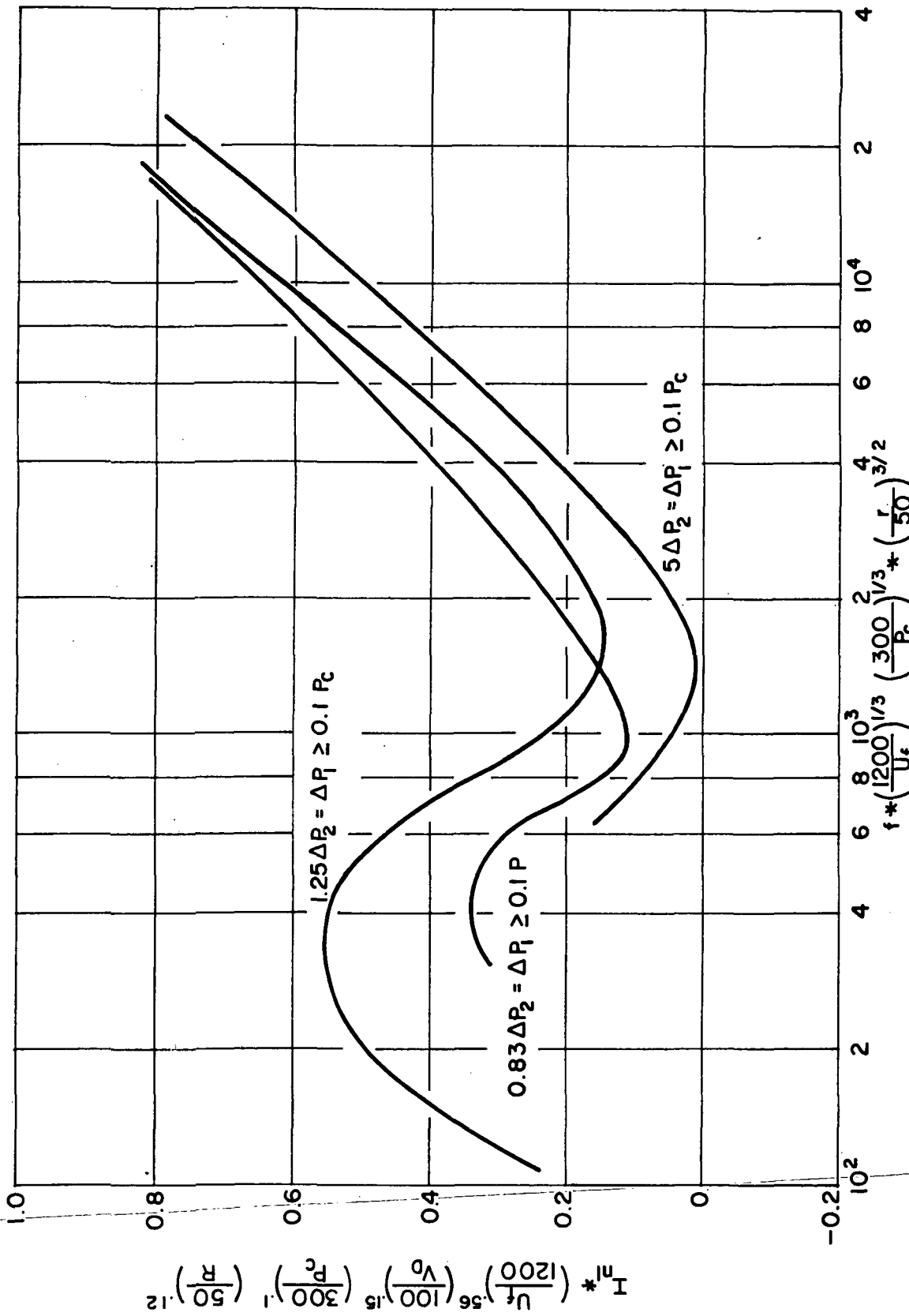


FIG. 10 NON-LINEAR OUT OF PHASE RESPONSE FACTOR VS. FREQUENCY FACTOR

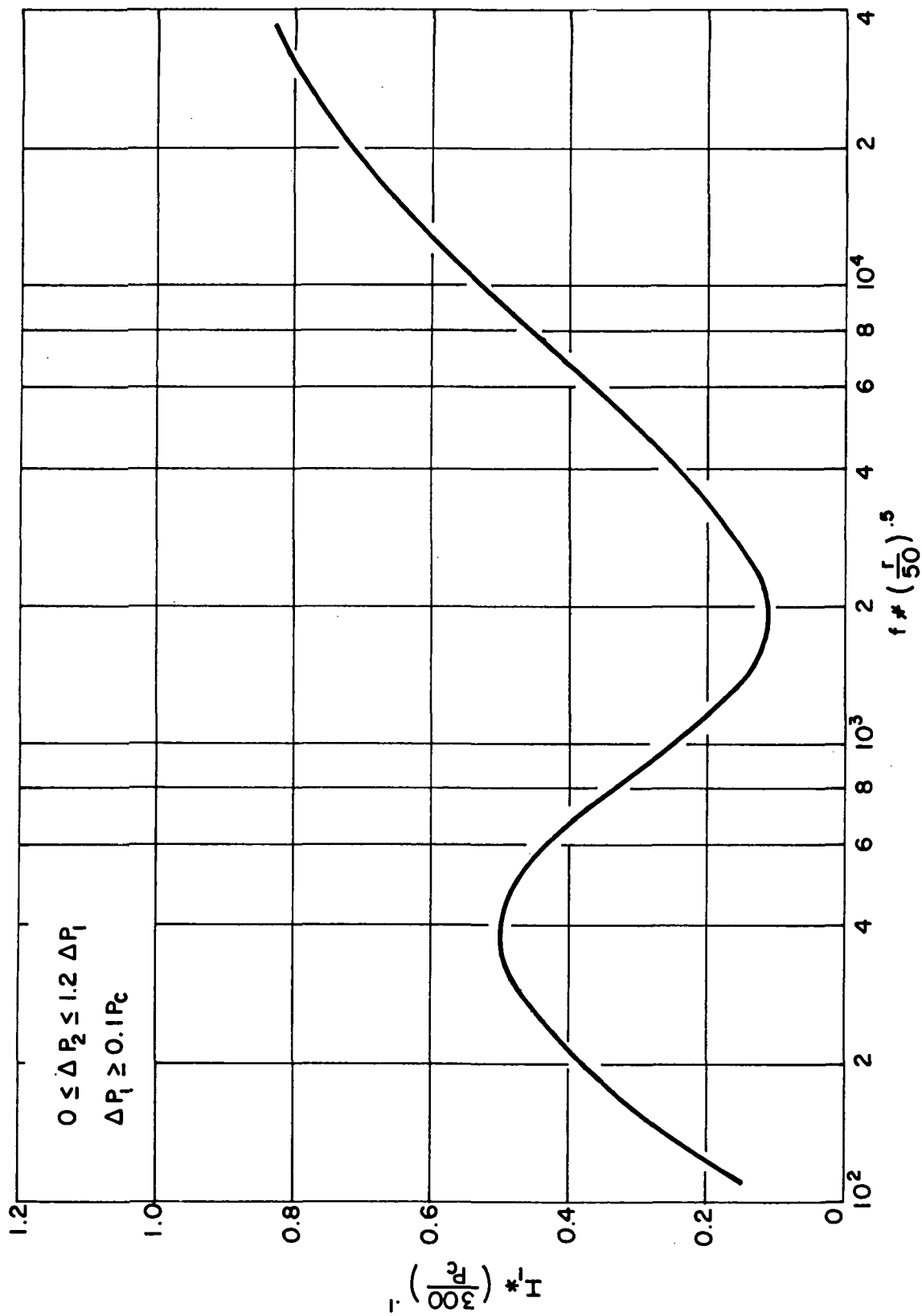


FIG. 11 FUNDAMENTAL OUT OF PHASE RESPONSE FACTOR VS. FREQUENCY FACTOR

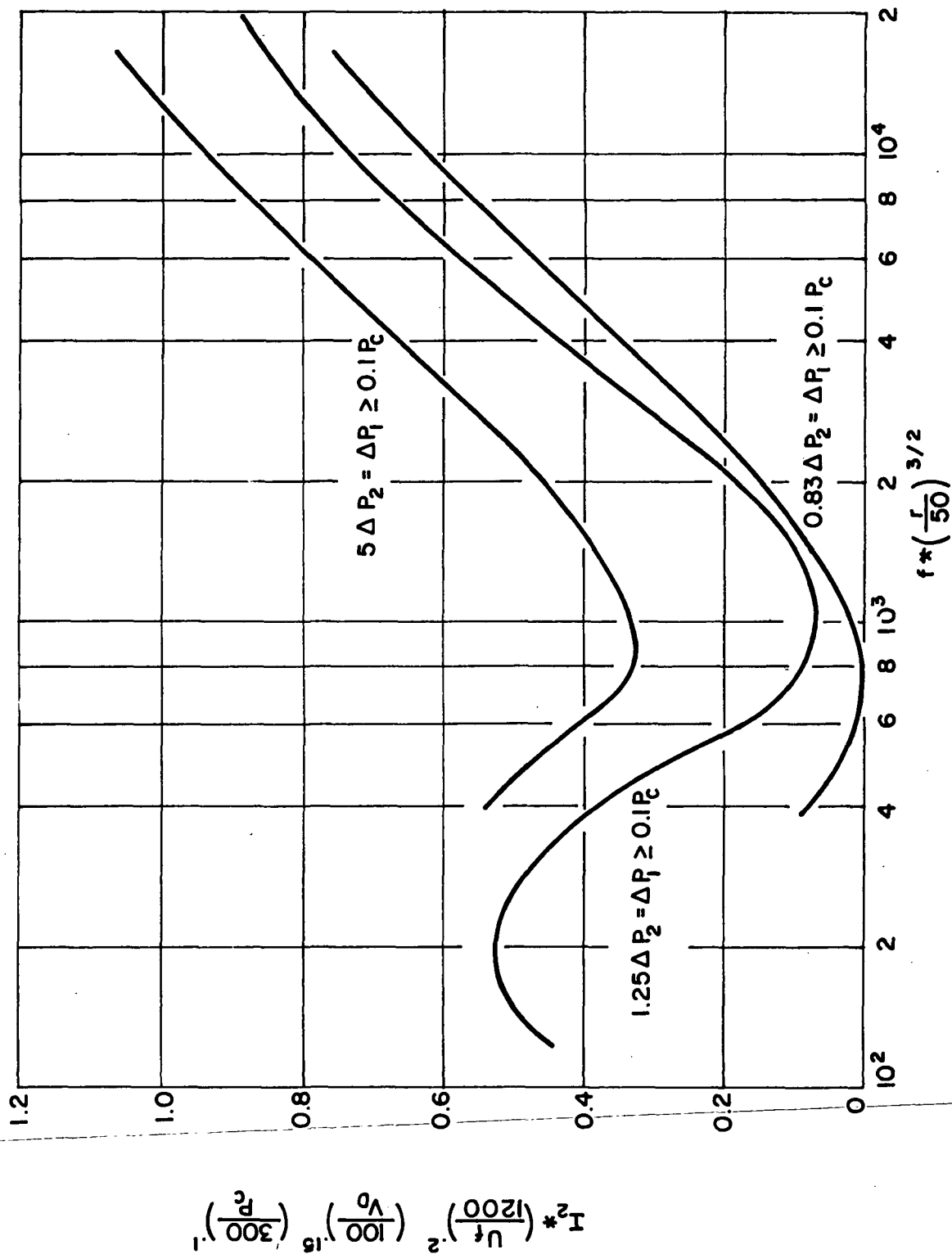


FIG. 12 FIRST HARMONIC OUT OF PHASE RESPONSE FACTOR VS. FREQUENCY FACTOR

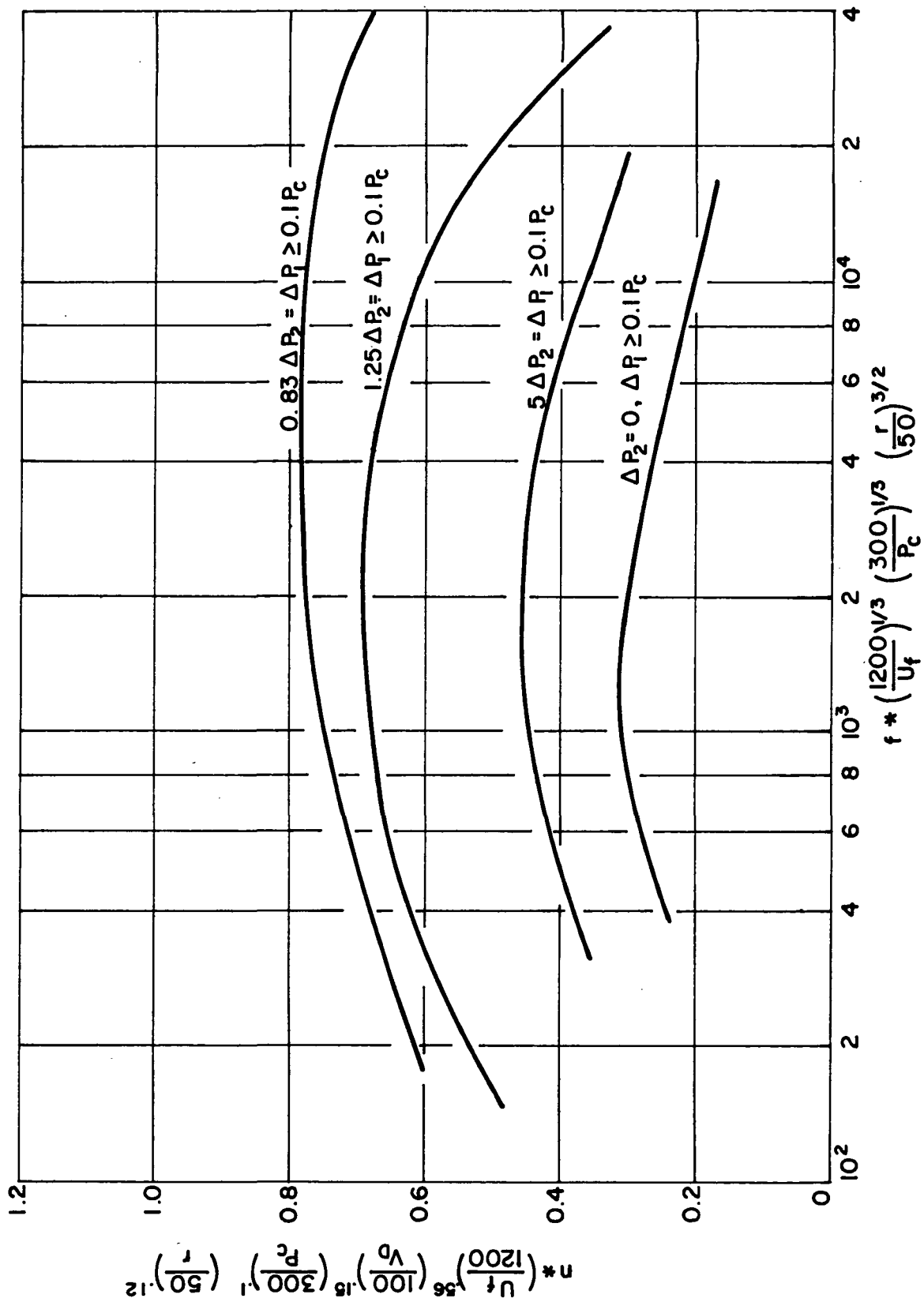


FIG. 13 "n" VS. FREQUENCY FACTOR

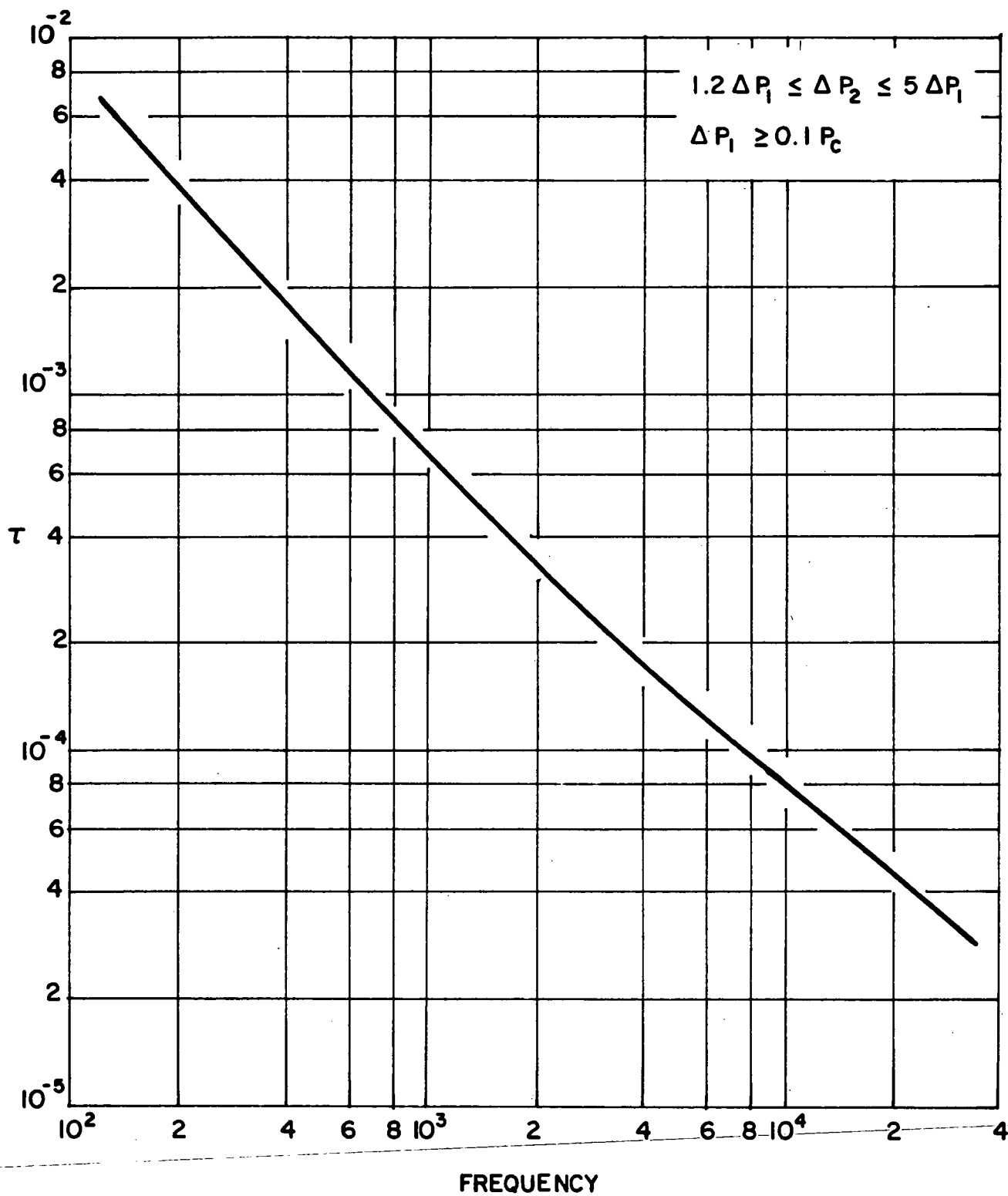


FIG. 14 τ VS. FREQUENCY



POSTMASTER: If Undeliverable (Section 158
Postal Manual) Do Not Return

"The aeronautical and space activities of the United States shall be conducted so as to contribute . . . to the expansion of human knowledge of phenomena in the atmosphere and space. The Administration shall provide for the widest practicable and appropriate dissemination of information concerning its activities and the results thereof."

—NATIONAL AERONAUTICS AND SPACE ACT OF 1958

NASA SCIENTIFIC AND TECHNICAL PUBLICATIONS

TECHNICAL REPORTS: Scientific and technical information considered important, complete, and a lasting contribution to existing knowledge.

TECHNICAL NOTES: Information less broad in scope but nevertheless of importance as a contribution to existing knowledge.

TECHNICAL MEMORANDUMS: Information receiving limited distribution because of preliminary data, security classification, or other reasons. Also includes conference proceedings with either limited or unlimited distribution.

CONTRACTOR REPORTS: Scientific and technical information generated under a NASA contract or grant and considered an important contribution to existing knowledge.

TECHNICAL TRANSLATIONS: Information published in a foreign language considered to merit NASA distribution in English.

SPECIAL PUBLICATIONS: Information derived from or of value to NASA activities. Publications include final reports of major projects, monographs, data compilations, handbooks, sourcebooks, and special bibliographies.

TECHNOLOGY UTILIZATION PUBLICATIONS: Information on technology used by NASA that may be of particular interest in commercial and other non-aerospace applications. Publications include Tech Briefs, Technology Utilization Reports and Technology Surveys.

Details on the availability of these publications may be obtained from:

SCIENTIFIC AND TECHNICAL INFORMATION OFFICE

NATIONAL AERONAUTICS AND SPACE ADMINISTRATION

Washington, D.C. 20546